eISSN: 2791-8742
doi: 10.52460/src

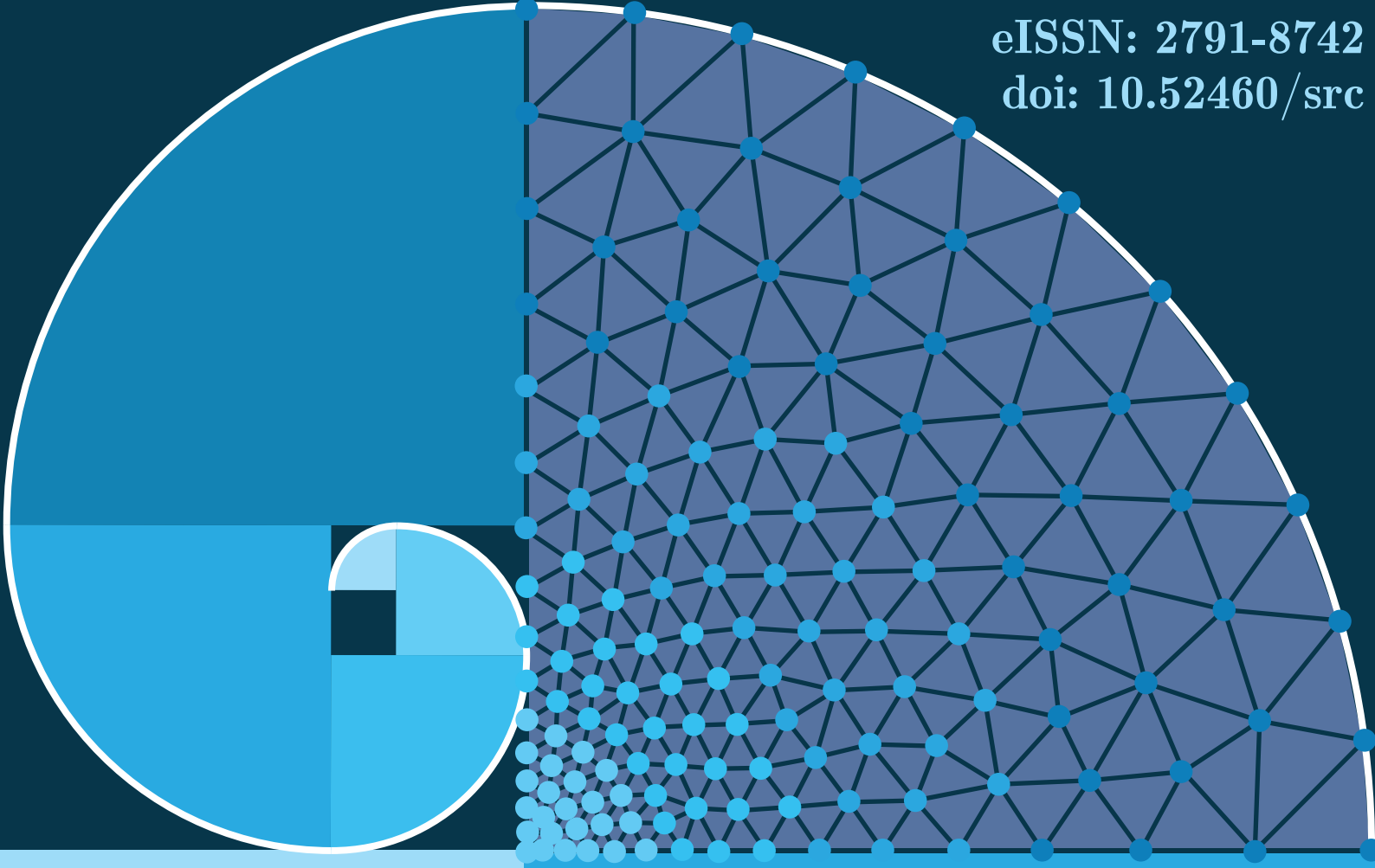

Scientific Research Communications

Volume 2
Issue 2
July 2022

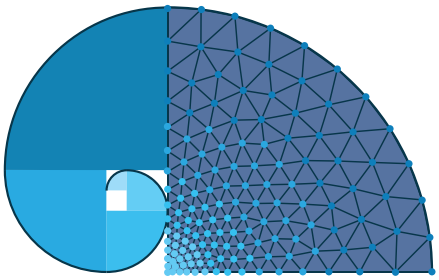

Scientific Research Communications
Volume 2, Issue 2, 2022

Editorial

Publisher
Prof. Dr. Mehmet ÇEVİK
İzmir International Guest Students Association

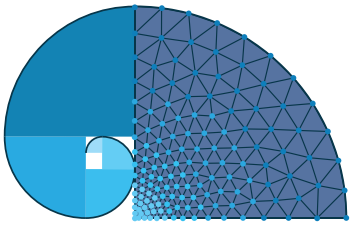

Scientific Research Communications

Volume 2, Issue 2, 2022

Contents

Research Articles

Scientific Research Communications

Research Article

Sci. Res. Comm. (2022)
Volume 2, Issue 2
doi: 10.52460/src.2022.006

Drought Class Probability Analysis for the Küçük Menderes River Basin

Serbay Tatar[1] **Ebru Eris**[2*]

[1] Izmir Metropolitan Municipality, Mimar Sinan District, 9 Eylul Square No: 9/1, Hall No. 1 in Kültürpark, Konak-Izmir, Türkiye
[2] Ege University, Civil Engineering Department, Bornova-Izmir, Türkiye
[*] Corresponding author: ebru.eris@ege.edu.tr

Received: 23.03.2022 Accepted: 22.07.2022

Abstract

Drought is a complex natural hazard that may take many years to develop and that has significant effects on human life, environmental systems, and the economy. Its impacts may also be serious and costly. This study, considering the fact that drought is a significant natural disaster, aimed to investigate the characteristics of drought in the Küçük Menderes River Basin. Among several drought indices, the Standardized Precipitation Index (SPI) and Streamflow Drought Index (SDI) were used for drought analysis. SPI and SDI were applied to the monthly precipitation data of Selçuk and Ödemiş meteorological stations with nos. 17854 and 17822, and to the monthly flow data of Selçuk and Bülbüller flow gauging stations with nos. E06A001 and D06A012, respectively. Drought classes for each month were obtained through the referred drought indices. Using the drought classes, meteorological and hydrological droughts were statistically investigated at a regional scale by determining the drought classes' occurrence probabilities, the expected residence time in each drought severity class, the expected first transition time, and the drought class with the highest probability of occurrence in the near future.

Keywords: Drought classes, transition probability, standardized precipitation index, streamflow drought index, Küçük Menderes River Basin

1. Introduction

Drought is a natural event that occurs when the amount of rainfall falls below its normal level, causing serious hydrological imbalances and negatively impacting land resources and production systems. Drought characteristics can be divided into four categories: frequency, severity, duration, and impact area. The drought's main characteristics include the uncertainty of its beginning and end, its cumulative increase in intensity, its impact on multiple resources at the same time, and its significant economic dimension (Turkes, 2010). A universal definition of drought is difficult to come up with. However, drought can be classified into four categories that are widely accepted. Droughts are classified as meteorological, agricultural, hydrological, and socioeconomic (Wilhite & Glantz, 1985). The frequency of possible drought events is of importance in terms of meteorology, hydrology, and agriculture.

In Douro, Portugal, 3- and 6-month scales' Standardized Precipitation Index (SPI3 and SPI6, respectively) values were considered for short-term and medium-term drought analysis. However, for the long-term analysis, the Markov chain approach was used. The expected residence time in each severity class, the expected first transition time, the recurrence time, and the class prediction on a short-term basis were also calculated. When examining the results of a drought event, SPI6 could have been preferred over SPI3, since the first indicated a higher persistence for the same class, being a better guarantee of less water scarcity when adequately managed (Abreu et al., 2008).

In the Eastern Mediterranean region, using the extensive annual and monthly rainfall time series of meteorological observation stations, the distribution among the drought categories of "mild, moderate, severe, and extreme" was determined through the SPI method, and the probability values of drought and deluge in different periods were calculated with the Markov chain. When analyzed spatially, it was determined that as the consecutive periods (1, 3, 6, 12, 24, or 48 months) increased, the probability of drought increased while the probability of deluge decreased in the study area (Fidan, 2011).

Another research aimed to examine and determine drought through the SPI by using monthly total precipitation and probabilities of being dry on the monthly scale with a 2-state first-order Markov chain approach in the Southeastern Anatolia Project (GAP) area. At the regional scale, results showed that a 50% or higher probability of drought was expected 99% of the project area. According to this study and the findings, agriculture-based industries were assessed for risk management (Tonkaz, 2008). In another study by Yildirim and Aksoy (2019), using the SPI, the drought classes' probabilities, the expected residence time in each drought class, the expected first transition time, and the drought class with the highest probability of occurrence in the near future were determined for the Akhisar meteorology station in the Gediz Basin, Turkey.

Nowadays, Turkey is facing problems such as water scarcity, sea level rise, drought, and floods. Droughts are becoming more common in many areas, particularly in areas that are important for national agriculture. İzmir, one of Turkey's major cities, is also at risk, and all cities rely on available fresh water in reservoirs (FAO, 2017; OECD, 2019). Forty-six percent of the İzmir province's surface water presence is in the Küçük Menderes River Basin. In the referred river basin, significant agricultural activities are being carried out with irrigation facilities, which increases water demand. It has therefore been an important study area for which water allocation and drought management plans have recently been prepared by state-owned organizations (TUBITAK, 2010; GDWM, 2016, 2017, Eris et al., 2020). In this study, the Küçük Menderes River Basin was selected as the study area.

Many studies on drought have been conducted in various parts of the world, including Turkey. However, the studies for the determination of transition probabilities from a given drought class to another are limited, particularly for any region in Turkey. The aim of this study was to determine the transition possibilities of drought classes, and thus to make short- and medium-term forecasts of drought transition based on the current state. For this purpose, the Streamflow Drought Index (SDI) was used in addition to the SPI in order to consider both meteorological and hydrological drought. The SPI and SDI were calculated using monthly precipitation for Selçuk and Ödemiş and flow data for Selçuk and Büllbüller, located in the Küçük Menderes River Basin. Drought classes were determined for each month. The drought classes' occurrence probabilities, the expected residence time in each class of severity, the expected first transition time, and the short-term drought class prediction were examined, and the relationship between meteorological and hydrological drought was tried to be determined.

2. Study Area and Method

The Küçük Menderes River Basin, a part of the administrative Küçük Menderes Basin (with no 06 in Figure 1) in the Aegean Region, in the western part of Turkey, was selected for the case study. The river basin has the characteristics of the Mediterranean climate. The winters are warm and rainy, while the summers are hot and dry. The long-term mean annual precipitation is approximately 600 mm, which corresponds to an 11.45 m^3/s annual average discharge at the outlet of the river basin (GDWM, 2016). For the analysis, the monthly precipitation data of Selçuk and Ödemiş meteorological stations (Station Nos. 17854 and 17822) and the flow data of the Selçuk and Bülbüller flow gauging stations (Station Nos. E06A001 and D06A012) located in the basin were obtained from the Directorate General for State Hydraulic Works (DSI) and the Turkish State Meteorological Service (MGM), and their particulars are given in Table 1.

Table 1. Meteorological and flow gauging stations in the Küçük Menderes River Basin

Meteorological station		Flow gauging station	
Station No	17854	Station No	E06A001
Station Name	Selçuk	Station Name	Selçuk
Coordinates	37° 56′ 32″ N,27° 22′ 01″ N	Coordinates	37° 58′ 45″ N, 27° 22′ 46″ E
Elevation (m)	18	Elevation (m)	4
Observation Period*	1964-2018	Observation Period*	1961-2008
Mean precipitation (mm)	570	Mean flow (m^3/s)	9.30
Station No	17822	Station No	D06A012
Station Name	Ödemiş	Station Name	Bülbüller
Coordinates	38° 12′ 57″ N, 27°57′ 52″ E	Coordinates	38° 13′ 54″ N, 27° 50′ 02″ E
Elevation (m)	111	Elevation (m)	130
Observation Period*	1960-2018	Observation Period*	1985-2002
Mean precipitation (mm)	438	Mean flow (m^3/s)	0.23

**Observation period shows the data range used in the study.*

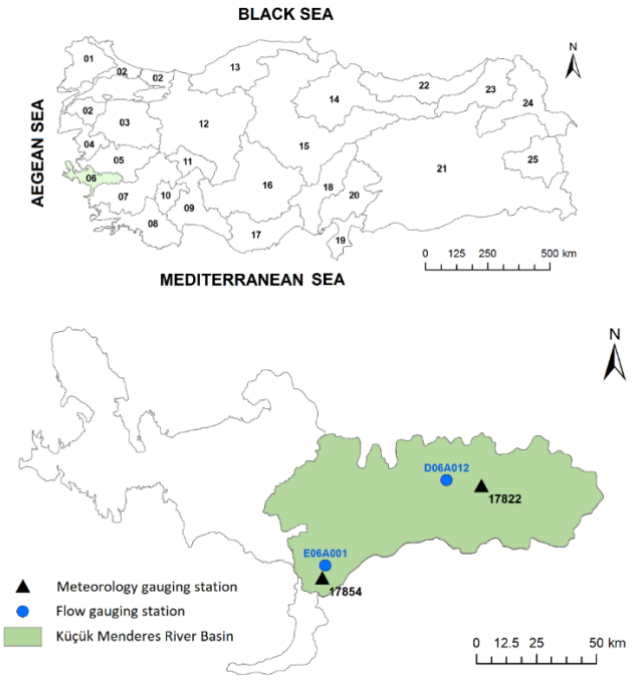

Figure 1. The locations of meteorological and flow gauging stations used in the study

2.1 Standardized Precipitation Index (SPI)

For meteorological drought analysis, the Standardized Precipitation Index (SPI) was used in this study. SPI is the most commonly used index to monitor and characterize meteorological droughts. SPI was developed by McKee et al. (1993), and described in detail by Edwards and McKee (1997). It measures precipitation anomalies for a location based on the comparison of observed total precipitation amount for an accumulation period of interest (e.g. 1, 3, 6, 9, 12, or 48 months) with the long-term historic precipitation record for that period. SPI1 and SPI3 (for 1- and 3-month scales) can be used as an indicator for immediate impacts such as reduced soil moisture, snowpack, and flow in smaller creeks. SPI6 and SPI9 can be used as indicators for reduced stream flow and reservoir occupancy, whereas SPI12, SPI24, and SPI48 can be used for reduced reservoir occupancy and groundwater recharge. Drought classifications based on the SPI values are given in Table 2.

Table 2. SPI/SDI Values of Drought Classifications

SPI /SDI Value	Classification
SPI/SDI≥ 0	Wet
0 < SPI/SDI < -1.0	Mild Drought
-1.0 ≤ SPI/SDI < -1.5	Moderate Drought
-1.5 ≤ SPI/SDI < -1.99	Severe Drought
SPI/SDI ≤ -2.0	Extreme Drought

2.2 Streamflow Drought Index (SDI)

In order to characterize hydrological drought, Nalbantis & Tsakiris (2009) developed the SDI by considering monthly streamflow value (Q_{ij}), where i is the hydrological year and j is the number of months in the hydrological year, based on the concepts of developing the SPI. The cumulative streamflow volume is given in Eq. (1):

$$V_{i,k} = \sum_{j=1}^{3k} Q_{i,j} \qquad i=1, 2, \ldots \quad j=1, 2, \ldots \quad k=1, 2, 3, 4 \tag{1}$$

where Vi,k is the cumulative streamflow volume for the ith hydrological year and for the kth reference period, and k=1 for October-December, k=2 for October-March, k=3 for October-June, and k=4 for October-September (as SDI1, SDI2, SDI3, SDI4).

The *SDI,* based on cumulative streamflow volumes ($V_{i,k}$) for each reference period k of the ith hydrological year, is defined as in Eq. (2):

$$SDI_{i,k} = \frac{V_{i,k} - V_k}{\sigma} i=1, 2, \ldots \; k=1, 2, 3, 4 \tag{2}$$

where V_k is the mean and σ is the standard deviation of the cumulative streamflow volumes of the reference period k. The states of hydrological drought based on SDI values are also given in Table 2.

2.3 Drought Class Probability

In determining the probability of drought classes, the following definitions, which were previously proposed and applied to different stations in the South of Portugal by Paulo & Pereira (2007), were used in this study:

Drought class probability is the possibility of occurrence of different drought classes;

Expected residence time in each drought class is the average time spent before transiting from the specified drought class to another class, and it represents the length of such a drought class;

The expected first transition time is the average time elapsed to reach the non-drought (wet) state from the specified drought class;

The drought class most likely to occur in the near future; the drought class most likely to be seen 1, 2, and 3 months following the relevant drought class.

3. Results and Discussion

SPI12 values were obtained for meteorological drought, and SDI4 values were obtained for hydrological drought regarding the Selçuk meteorological and flow gauging stations. Based on the SPI12 and SDI4 time series, the drought class probabilities, the expected residence time in each drought class, the expected first transition time, and the drought class with the highest probability of occurrence in 1, 2, and 3 months following the relevant drought class were determined for each station.

When the SPI12 values (Table 3) were examined, Selçuk meteorological station came up as the one where the highest "mild-drought" was occurring with 245 months, and the probability of occurrence was calculated as 37.8%. "Mild drought" occurred at Ödemiş meteorological station for 237 months, with a probability of occurrence of 34.0%. Since SPI classification is suitable for normal distribution due to its calculation method, the probability of the occurrence of "mild drought" classes close to the average was high. As the drought severity increases, the number of incidents, and therefore, the probability of the occurrence of drought, decreases. The drought class least likely to occur was the "extreme drought" class, with 0.020 and 0.025 for both stations, respectively.

Table 3. Drought class probabilities for SPI12

Drought Class	SELÇUK Station (17854)		ÖDEMİŞ Station (17822)	
	Number of Occurrence	Probability of Occurrence	Number of Occurrence	Probability of Occurrence
Extreme Drought	16	0.025	14	0.020
Severe Drought	30	0.046	42	0.060
Moderate Drought	43	0.066	59	0.085
Mild Drought	245	0.378	237	0.340
Non-Drought	315	0.485	345	0.495

On the other hand, as per SDI4 values (Table 4), "mild drought" class with 164 and 56 months occurred as the drought class with the highest number, and the probability of its occurrence was calculated as 29.0% for Selçuk and Bülbüller flow gauging stations. As SDI is basically the conversion of the streamflow time series to the standard normal distribution, the probability of the occurrence of "mild drought" classes close to average was high. Just like SPI12, as the severity increases, the number of incidents, and therefore, the probability of the occurrence of drought, decreases. The drought classes least likely to occur were the "extreme drought" class with a probability of 0.027 for Selçuk flow gauging station and the "severe drought" class with a probability of 0.026 for Bülbüller flow gauging station.

In terms of expected residence time in each drought class, 12-month droughts tended to take approximately 1.5 and 5.2 months between the "moderate drought" and "mild drought" classes at Selçuk meteorological station (Table 5), and they tended to take approximately 2.0 and 4.6 months between the "moderate drought" and "mild drought" classes at Ödemiş meteorological station.

Table 4. Drought class probabilities for SDI4

Drought Class	SELÇUK Station (E60A001)		BÜLBÜLLER Station (D06A012)	
	Number of Occurrence	Probability of Occurrence	Number of Occurrence	Probability of Occurrence
Extreme	15	0.027	10	0.052
Severe Drought	31	0.055	5	0.026
Moderate	34	0.060	17	0.088
Mild Drought	164	0.290	56	0.290
Non-Drought	321	0.568	105	0.544

Table 5. Expected residence time for SPI12

Drought Class	SELÇUK Station (17854)	ÖDEMİŞ Station (17822)
	Expected Residence Time	
Extreme Drought	3.2	3.5
Severe Drought	2.0	2.2
Moderate Drought	1.5	2.0
Mild Drought	5.2	4.6

In terms of hydrological drought, 12-month droughts generally tend to take quite a long time compared to meteorological droughts. While the residence time in the drought period changed between 3.4-15.0 months at Selçuk flow gauging station, it changed between 1.7-10.0 months at Bülbüller flow gauging station (Table 6). When Tables 5 and 6 are considered together, it can be said that hydrological drought has a more persistent characteristic compared to meteorological drought.

Table 6. Expected residence time for SDI4

Drought Class	SELÇUK Station (E60A001)	BÜLBÜLLER Station (D60A012)
	Expected Residence Time	
Extreme	15.0	10.0
Severe Drought	7.8	1.7
Moderate	3.4	5.7
Mild Drought	9.6	5.1

As seen in Table 7, the first "wet" period was observed in 20.9-41.0 months following a dry period of "extreme drought", "severe drought", "moderate drought", and "mild drought" classes at Selçuk meteorological station. The first "non-drought" period was observed in 16.0-22.9 months following a dry period of "extreme drought", "severe drought", "moderate drought", and "mild drought" classes at Ödemiş meteorological station.

Table 7. Expected first transition time for SPI12

Drought Class	SELÇUK Station (17854)	ÖDEMİŞ Station (17822)
	The Expected First Transition Time	
Extreme Drought	36.6	16.0
Severe Drought	41.0	21.0
Moderate Drought	40.0	22.9
Mild Drought	20.9	17.1

The first wet period was observed in 75 months after a long period following a dry period of "extreme drought" class at Selçuk flow gauging station. In terms of "mild drought" class, the expected first transition time generally increased as the drought severity increased (Table 8). The first wet period was observed in 15 months following a dry period of "extreme drought" class for Bülbüller flow gauging station. For both stations, in terms of "extreme drought" class, the expected first transition time generally decreased as the drought severity decreased. Like the results of "the expected residence time", the results of "the expected first transition time" showed that the transition from a drought class to a wet state takes longer in the hydrological aspect compared to the meteorological aspect. Another conclusion derived from Tables 7 and 8 is that the results of "the expected first transition time" were higher for Selçuk meteorological and flow gauging stations compared to Ödemiş meteorological station and Bülbüller flow gauging station. Selçuk meteorological and flow gauging stations are located at the southwest, whereas the others are at the northeast part of the region. Spatially, these results suggest that the southwestern part of the region transits from a drought class to the wet state in a longer period compared the northeastern part of the region.

Table 8. Expected first transition time for SDI4

Drought Class	**SELÇUK Station (E60A001)**	**BÜLBÜLLER Station (D60A012)**
	The Expected First Transition Time	
Extreme Drought	75.0	15.0
Severe Drought	53.3	7.7
Moderate Drought	55.4	7.0
Mild Drought	34.4	8.4

The aim of the study was also to predict future drought conditions with the help of current drought conditions. Accordingly, the drought class with the highest probability of occurrence in the near future was determined. The drought classes most likely to occur in 1, 2, and 3 months following other drought classes were determined, and they are shown in Tables 9-12 as per SPI12 and SDI4, respectively. In terms of all the drought classes, the most probable classes that occurred in the 1-3 months following them were again the same.

Table 9. SPI12 the drought class most likely to occur in the near future at SELÇUK meteorological station (17854)

	1 Month Later		**2 Months Later**		**3 Months Later**	
Drought Class	Most Probable Drought Class	Probability of Occurrence	Most Probable Drought Class	Probability of Occurrence	Most Probable Drought Class	Probability of Occurrence
Wet	Wet	0.92	Wet	0.87	Wet	0.83
Mild D.	Mild D.	0.81	Mild D.	0.74	Mild D.	0.68
Moderate	Moderate	0.44	Moderate D.	0.51	Moderate D.	0.53
Severe D.	Severe D.	0.50	Severe D.	0.40	Severe D.	0.27
Extreme D.	Extreme D.	0.69	Extreme D.	0.50	Extreme D.	0.31

Table 10. SPI12 the drought class most likely to occur in the near future at ÖDEMİŞ meteorological station (17822)

	1 Month Later		2 Months Later		3 Months Later	
Drought Class	Most Probable Drought Class	Probability of Occurrence	Most Probable Drought Class	Probability of Occurrence	Most Probable Drought Class	Probability of Occurrence
Wet	Wet	0.91	Wet	0.87	Wet	0.84
Mild D.	Mild D.	0.78	Mild D.	0.69	Mild D.	0.64
Moderate	Moderate	0.49	Moderate	0.44	Moderate D.	0.42
Severe D.	Severe D.	0.55	Severe D.	0.43	Severe D.	0.38
Extreme D.	Extreme D.	0.71	Extreme D.	0.57	Extreme D.	0.50

Table 11. SDI4 the drought class most likely to occur in the near future at SELÇUK flow gauging station (E60A001)

	1 Month Later		2 Months Later		3 Months Later	
Drought Class	Most Probable Drought Class	Probability of Occurrence	Most Probable Drought Class	Probability of Occurrence	Most Probable Drought Class	Probability of Occurrence
Wet	Wet	0.97	Wet	0.95	Wet	0.93
Mild D.	Mild D.	0.90	Mild D.	0.83	Mild D.	0.76
Moderate	Moderate	0.71	Moderate	0.56	Moderate D.	0.44
Severe D.	Severe D.	0.87	Severe D.	0.74	Severe D.	0.61
Extreme D.	Extreme D.	0.93	Extreme D.	0.87	Extreme D.	0.80

Table 12. SDI4 the drought class most likely to occur in the near future at BÜLBÜLLER flow gauging station (D60A012)

	1 Month Later		2 Months Later		3 Months Later	
Drought Class	Most Probable Drought Class	Probability of Occurrence	Most Probable Drought Class	Probability of Occurrence	Most Probable Drought Class	Probability of Occurrence
Wet	Wet	0.91	Wet	0.87	Wet	0.81
Mild D.	Mild D.	0.80	Mild D.	0.70	Mild D.	0.61
Moderate	Moderate	0.82	Moderate	0.76	Moderate	0.65
Severe D.	Severe D.	0.40	Severe D.	0.40	Severe D.	0.40
Extreme D.	Extreme D.	0.90	Extreme D.	0.80	Extreme D.	0.70

4. Conclusions

The drought classes' occurrence probabilities, the expected residence time in each drought severity class, the expected first transition time, and the drought class with the highest probability of occurrence in the near future were evaluated for meteorological and hydrological droughts in the Küçük Menderes River Basin. According to the results, the following conclusions can be drawn:

- The probability of drought decreases as the severity of the drought increases during the observation period.
- The probability of "extreme drought" at both stations was 2.0%-2.5% and 2.7%-5.2% for SPI12 and SDI4, respectively. Due to the normal distribution of SPI and SDI,

extreme values were unlikely to be seen. Therefore, a low probability of "extreme drought" was expected.

- The expected residence time in each drought severity class was longer in terms of hydrological drought (SDI4) compared to meteorological drought (SPI12). There was persistent "extreme drought", particularly in terms of hydrological drought. In other words, hydrological drought has a more persistent character compared to meteorological drought. This result is important, and it should be emphasized in terms of measures to be taken against drought.
- The results of the expected first transition time showed that the transition from a drought class to a non-drought state takes longer in the hydrological aspect compared to the meteorological aspect. Due to the location differences of the meteorological and flow gauging stations, spatially, the results showed that the southwestern part of the region transits from a drought class to a non-drought state in a longer period compared to the northeastern part of the region. However, this fact needs to be proven through more stations.
- In terms of all the drought classes, the most probable classes that occurred in 1, 2, and 3 months following them were again the same. When the expected residence times and the first transition times were examined, it was concluded that the hydrological drought lasts longer than the meteorological drought. According to these results, the most likely situations in 1, 2, or 3 months can be considered as drought prediction tools for transitions among drought severity classes.

For future studies, more precipitation and flow data from meteorological and flow gauging stations can be obtained to evaluate the drought characteristics of the Küçük Menderes River Basin accurately. The Markov chain can be used in order to model SPI transition classes for better understanding the drought characteristics of the study region. Drought transition probabilities may also be calculated for different drought indices (Palmer Drought Severity Index, PDSI; Standardized Precipitation Evapotranspiration Index, SPEI, etc.).

Author Statement

The authors confirm their contribution to the paper as follows: study conception and design: E. Eris; data collection: S. Tatar; analysis: S. Tatar; interpretation of results and draft manuscript preparation: S. Tatar, E. Eris. All authors reviewed the results and approved the final version of the manuscript.

Conflict of Interest

The authors declare no conflict of interest.

References

Abreu, I., Guerreiro, M.J., & Lajinha, T. (2008). A stochastic approach to standardized precipitation index class transitions. *Revista da Faculdade de Ciência e Tecnologia*. 1. 40-53.

Edwards, D.C., & McKee, T.B. (1997). Characteristics of 20th Century Drought in the United States at Multiple Times Scales. *Atmospheric Science Paper*, 634, 1-30.

Eris, E., Cavus, Y., Aksoy, H., Burgan, H. I., Aksu, H., & Boyacioglu, H. (2020). Spatiotemporal analysis of meteorological drought over Kucuk Menderes River Basin in the Aegean

Region of Turkey. *Theoretical and Applied Climatology*. 142, 1515–1530, https://doi.org/10.1007/s00704-020-03384-0.

FAO, Food and Agriculture Organization of United Nations (2017). Drought characteristics and management in Central Asia and Turkey. FAO Water Reports No.44. Rome, 114p.

Fidan, İ.H. (2011). Drought Analysis by Standardized Precipitation Index (SPI) and Determination of Drought Occurrence Probabilities through Using Markov Chains in the Eastern Mediterranean Region, MSc Thesis, Çukurova University, Institute of Natural and Applied Sciences, Adana (in Turkish).

GDWM (2016). Impact of Climate Change on Water Resources, Final Report, Appendix 8 – Küçük Menderes River Basin, General Directorate of Water Management (Iklim Değişikliğinin Su Kaynaklarina Etkisi, Proje Nihai Raporu, Ek 8 – Küçük Menderes Havzası, Su Yönetimi Genel Mudurlugu) Ankara (in Turkish).

GDWM (2017). Preparation of Water Allocation Plans for Küçük Menderes and Gediz Basins, General Directorate of Water Management (Küçük Menderes ve Gediz Havzası Su Tahsis Planlarının Hazırlanması, Su Yönetimi Genel Müdürlüğü) Ankara (in Turkish).

McKee, T. B., Doesken, N. J., & Kleist, J. (1993). The relationship of drought frequency and duration to time scales, In: Proceedings of the 8th Conference on Applied Climatology, Anaheim, CA, USA, pp 179–184.

Nalbantis, I., & Tsakiris, G. (2009). Assessment of hydrological drought revisited. *Water Resources Management*, 23(5), 881–897. https://doi.org/10.1007/s11269-008-9305-1

OECD (2019). OECD Environmental Performance Reviews: Turkey 2019, OECD Environmental Performance Reviews, OECD Publishing, Paris, https://doi.org/10.1787/9789264309753-en.

Paulo , A. A., & Pereira, L. S. (2007). Prediction of SPI drought class transitions using Markov chains. *Water Resources Management*, 21(10), 1813-1827. https://doi.org/10.1007/s11269-006-9129-9

Tonkaz, T. (2008). Drought Analysis Using First Order Markov Chaın in Southeastern Anatolia Project Area. *Journal of the Faculty of Agriculture of Harran University*, 12(1), 13 - 18 (in Turkish).

TUBITAK (2010). Water Management and Preparation of Basin Protection Action Plans. The Scientific and Technological Research Council of Turkey (TUBITAK)-Marmara Research Center (MAM) (Havza Koruma Eylem Planları – Küçük Menderes Havzası, TÜBİTAK-Marmara Araştırma Merkezi), Ankara (in Turkish).

Turkes, M. (2010). Climatology and Meteorology. First Edition, Kriter Publisher – Publication No. 63, Physical Geography Series No. 1, ISBN: 978-605-5863-39-6, 650 + XXII pp., İstanbul (in Turkish).

Wilhite, D.A., & Glantz, M.H. (1985). Understanding the Drought Phenomenon: The Role of Definitions. *Water International*, 10(3), 111–120.

Yildirim, I., & Aksoy H. (2019). Determination of SPI Drought Classes Transition Probabilities for Gediz River Basin. In: Proceedings of the 10th National Hydrology Congress, Muğla Sıtkı Koçman University (in Turkish).

Scientific Research Communications

Research Article

Sci. Res. Comm. (2022)
Volume 2, Issue 2
doi: 10.52460/src.2022.007

Conceptual Study of Non-Stick Cookware Coatings and the Effect of Some Corresponding Additives on Their Performance

Jabir Ismaeili[1,*] Jigneshkumar Patel[2] Bikem Övez[3]

[1,2] Kanat Paints and Coatings, Therna Subsidiary, R&D Dept., Izmir, Türkiye
[3] Ege University, Department of Chemical Engineering, Izmir, Türkiye
[*] Corresponding author: jabir.ismaeili@gmail.com

Received: 28.07.2022 Accepted: 23.08.2022

Abstract

In this study, the effect of some additives including Alumina (Al2O3), boron carbide (B4C), and different types of silicon carbide (SiC) on glossiness, impact resistance, pencil hardness, conical bent resistance, corrosion, humidity, and chemical resistance of non-stick coatings were studied. The results revealed that the glossiness of the coatings decrease by the addition of the additives, but the overall resistance of the coatings grow by adding these substances among which B4C additive had the best effect on the coating general performance.

Keywords: Non-stick coatings, cookware and bakeware, fluoropolymer, curing and sintering, mechanical strength

1. Introduction

Non-stick coatings are hydrophobic surfaces, which have low coefficients of friction. The most common material used in this industry is Poly Fluoro Carbon (PFC) polymers and particularly Poly Tetra Fluoro Ethylene (PTFE) because of its anti-stick characteristics, mechanical strength and low flammability could be taken into account as the best option for the non-stick industry. Besides the fluorocarbons, many other ingredients in non-stick cookware coating formulation play unique roles in the performance of the products which needs to be investigated in detail. Also, non-stick coatings are applied with different methods and the most common application methods are air spraying and roller methods. The fluorocarbon polymer coating preferably comprises a primer layer which is applied directly onto the surface of the substrate and one or more fluorocarbon polymer topcoat layers. An illustration of a non-stick coating has been shown in Figure 1. The performance of the coatings could be affected by many factors including the ingredients of the formulation, coating thickness, flash-off, and curing temperature and durations.

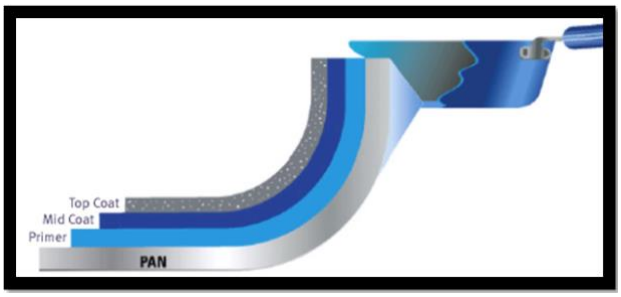

Figure 1. Coating layers of a non-stick cookware

1.1 Non-Stick Coatings

Non-stick coatings are hydrophobic surfaces, which have low coefficients of friction, high corrosion resistance, high dielectric strengths, higher temperature resistances compared to other polymers and a wide range of operational temperature. Fluoropolymers are among the oldest high-performance polymers and are of great commercial and scientific interest. Most of these are because of their anti-stick characteristics, mechanical strength, and low flammability. The most important disadvantage of PTFE is low wear resistance (Hatzikiriakos, 2012). Their most important uses are in electronics and electrical applications, chemical processing equipment, laboratory ware and tubing, material for roofing, and houseware (Ebnesajjad, 2015).

The term fluorocarbon polymer coating refers to a coating that is consist of conventional fluorocarbon polymers such as polytetrafluoroethylene (PTFE), polymers of chloro-tri-fluoroethylene (CTFE), fluorinated ethylene-propylene polymers (FEP), polyvinylidene fluoride (PVF), combinations thereof and the like. The composition of the fluorocarbon polymer coating is not critical, and a variety of fluorocarbon polymer compositions are conventionally used in the formulation of a non-stick coating. Non-stick coatings are plated with different methods like immersion, roller coating, thermal spray, curtain coating, and more are carried out in many ways. The most common coating method is the air spray method.

The PTFE with IUPAC ID: Poly (1, 1, 2, 2 tetrafluoroethylene) with the trade name of Teflon and (C2F4) n formula is a synthetic fluoropolymer compound, which was originally discovered by DuPont company in 1938. Today, Teflon™ coatings, and additives are used in paints, fabrics, carpets, home furnishings, clothing and so much. PTFE has one of the lowest coefficients of friction of any solid. It is non-reactive, partly because of the strength of carbon–fluorine bonds. PTFE application in cookware utensils has two important reasons: 1) being non-stick and 2) having a high thermal resistance. PTFE has excellent corrosion resistance, high-temperature resistance, anti-stick behavior, and low friction coefficient, widely used as an anti-corrosive material, sealing material, insulating material, non-sticky material, self-lubricating material, etc. (Lee et al., 2007; Beckford et al., 2016)

In the case of coatings, the fluorocarbon polymer coating preferably comprises a primer layer and one or more fluorocarbon polymer topcoats. The primer layer comprises a blend of fluorocarbon polymers and one or more adhesion promoting high-temperature binder resins, such as polyamide-imide resins (PAI), polyethersulfone resins (PES), and polyphenylene sulfide resins (PPS). PAI is an extremely strong and stiff plastic material. It is often used in elevated temperature environments where other thermoplastics would lose their mechanical properties (Yu et al., 2018). Polyethersulfone is an amorphous, transparent, and pale amber high-performance thermoplastic and is the most temperature-resistant transparent commercially available thermoplastic resin (McKeen, 2019). PPS is an engineering plastic,

commonly used today as a high-performance thermoplastic. The maximum service temperature for PPS is 218 °C. Synthetic fiber and textiles derived from this polymer resist chemical and thermal attacks (Ebnesajjad and Morgan, 2019). Cookware coating with long-term scratch resistance has always been a desirable feature for cooks. The coatings also add colour accents to the kitchen. The first component, the basic layer or primer, consists of the fluoropolymer PTFE with integrated ceramic reinforcement. The layer in direct contact with the food is a specialty high-performance polymer containing PTFE (Chemours, 2017). The primer layer is applied directly onto the surface of the substrate. The non-vitreous inorganic oxide particles in the layer of the substrate enrich the surface of the substrate with bonding sites for the binder resins in the primer, thus improving the adhesion of the applied fluorocarbon polymer coating to the substrate. After the primer layer is applied, one or more fluorocarbon polymer topcoats are typically applied by conventional wet or dry techniques and then the entire fluorocarbon polymer coating is sintered on 400 °C (Rossi et al., 2022).

The current total volume of fluoropolymers produced in the world is in excess of 200,000 tones. Based on 2007 information total volume of fluoropolymers produced atthat time was 90,000 tones valued at over US$2 billion. PTFE is by far the most widely used fluoropolymer, accounting for some 70% of the total.2 the current average annual growth is estimated to be about 4% and is predicted to be about 5%. The typical cost of fluoroplastics ranges from US$13 to 45 per kilogram. Fluoroelastomers are priced somewhat higher than fluoroplastics and specialty fluoropolymers may cost up to several thousand US dollars per kilogram. (Drobny, 2007; Drobny, 2020).

1.2 The Effects of Different Additives in Non-stick Coating

PTFE's anti-wear applications have been somewhat limited by its poor wear resistance, which has led to the failure of anti-wear parts and films. Therefore, many researchers have attempted to reinforce PTFE using various fillers (Lee et al., 2007). Additives are very important in non-stick subjects and their effect can be very helpful for the goals of any product. Beckford et al. (2014) examined the PTFE + Au composite and PTFE properties and compared them with each other to evaluate the Au additive effect. These results indicate that the PTFE film has a significantly higher surface roughness than PTFE + Au. This difference in surface roughness results from the higher degree of melting in the composite film, which allows the film to spread and produce a more even film by Au nanoparticles. Durability test results indicate that by incorporating Au nanoparticles, even at the low concentration of 0.06 wt. %, it is possible to improve the wear resistance of the PTFE film twofold. Dynamic coefficient of friction is also influenced that much. Then it is concluded that adding Au nanoparticles of approximately 15 nm diameters, at a very low concentration of 0.06 wt. %, significantly improves the tribological properties. Also, test results show that incorporating Au nanoparticles as a filler not only increased the film's wear resistance but also shows no sign of delamination or adhesive wear (Beckford et al., 2014). It is known that besides PTFE, polyamide-imide and polyether sulfone are applied for light cookware utensils too. In general, to increase abrasion and scratch resistance of Teflon, nano-sized ceramic and/or metallic-based coatings powders are mixed. Glass fibers, carbon fibers, and nonferrous metallic and ceramic powders were studied as potential fillers for the enhancement of the wear resistance of PTFE. The wear process in the composites depends mainly on three factors: thermal stability, thermal conductivity, and the characteristics of the filler materials. But it was proven that these fillers induced a large frictional coefficient and abrasion of the fractured fiber and also the glossiness of the coatings is affected by hardening additives (Khedkar et al., 2002; Tevrüz, 1998; Tevrüz, 1999; Cheng et al., 2002).

The effects of additives not only on fluorocarbons are investigated but also on other coatings. In a study that Abenojar et al. (2009) had done, two different B_4C particle sizes were used for reinforcing an epoxy resin: one with an average particle size of 7 mm and the other with 23 mm. The results show that the addition of B_4C did not affect the degree of conversion of the epoxy during the curing and shifted the glass transition temperature of the epoxy to lower values and also increased the abrasive wear of the material. Epoxy-B_4C composites showed excellent bending strength, increasing with B_4C content and with the smaller particles (Abenojar J, 2009). The commercial PTFE-based coatings were found to provide poor release properties due to the presence of surface micro-cracks, which allowed epoxide penetration when cured under elevated pressure and temperature (Critchlow et al., 2006). In the work of Critchlow et al. (2006), Electroless Ni/PTFE composite coatings comprise a hard nickel–phosphorus matrix containing a very fine dispersion of PTFE particles. The matrix proved sufficiently robust for industrial applications and the low friction and surface energy provided by the embedded PTFE combined with macroscopic-scale surface roughness provided efficient mold release. According to the results, the PTFE composites provide a wide water contact angle because of low friction and also provide low-energy surfaces on metal substrates. After evaluating both samples of these coatings for use with metal tooling materials, it was found that when adhesives were cured under elevated pressure and temperature whilst in contact with the coatings, the subsequent release was poor or impossible. It is proposed that the porosities present in PTFE surfaces allow penetration of the. It results in resistance against corrosion and humidity and also reducing of the glossiness. In another study investigation of the physical-mechanical properties of PTFE, which was filled with different amounts of various materials, was done. The method of study was determination of frictional thermal stability by using the friction machine. The results showed that friction of thermal stability is increased with rising additives ratio (Kutelia et al., 2015). Thomas (1998) in a study, which was done with different fluoropolymers such as PTFE, PFA and FEP, the non-stick coating sprayed on the steel without primer and at a film thickness of 13- 14 µm. The films were cured at 430 °C and then the friction properties of the film were measured. As expected, it has been seen that PTFE has the lowest coefficient of friction but poor wear and adhesion properties. PFA and FEP adhered very well to the substrate but had a higher coefficient of friction. The 50/50 blends at the beginning of the test had a coefficient of friction, which was close to that of pure PTFE showing that PTFE might stratify. As the cylinder penetrated the film, the coefficient of friction increased to a maximum value until the contact became partly metal to- metal (Thomas, 1998). As it is obvious from the literature review, the additives have very important and effective influences on the non-stick coatings. Based on these reasons, in the present study the effects of several hardening additives have been investigated.

1.3 Non-stick Coatings and Health Issue

While PTFE is stable and nontoxic at lower temperatures, it begins to get deteriorated after the temperature of cookware reaches about 260 °C and decomposes above 350°C. PTFE cookware is considered as an insignificant exposure pathway to Perfluorooctanoic acid but in recent years the use of PFOA got banned from cookware use and afterward these coatings were approved by FDA for use in food contact coatings.

2. Materials and Methods

2.1 Materials

All the materials and equipment of this work were granted by THERNA non-stick coating producer which is a brand of KANAT paints and Coatings Company. The coating used in this study was a non-stick coating consist of a primer layer which provides the adhesion to substrate and the topcoat which grant the non-stick properties to the surface. The materials to be used in this kind of coatings consist resins, solvents, pigments and additives. The materials of the primer layer were added in two main stages including co-grind (premix) and letdown stages. In co-grind stage the materials to premix were: PW, Co-solvent, Defoamer, Surfactant, Filler, and Pigment and various hardening materials including Al_2O_3, B_4C, Black and Green SiC types which was the main subject of this study. In the letdown stage following materials were added: Surfactant, Resin, pH adjuster, Rheological agent, PW. Topcoat was fixed for all of the experiments with a fixed formulation. Aluminum panels were used as the substrate of the coatings. Five groups of this study were differed with their hardening material. In the samples of first group any hardening material was not used to have a reference to general comparison of the samples. The groups labeled as Table 1.

Table 1. Five coating groups of the study

	G.1	G.2	G.3	G.4	G.5
Additive	Blank	Black SiC	B4C	Green SiC	Al2O3

2.2 Methods

The tests were performed for 5 groups of samples. These tests were glossiness, impact resistance, pencil hardness, conical bent resistance, corrosion, humidity and chemical resistance (against sulfuric acid (H_2SO_4) 10%, sodium hydroxide (NaOH) 25% and diesel).

2.2.1 The preparation of the panels

The process of application of the coatings on the Aluminum panel is involved of 7 stages including sandblasting (grinding), cleaning of the surface, primer application on the surface, a 5-minute flash off in a 150 °C oven, striking of the top-coat, curing process on 375-425 °C oven and cooling down the coated panels. The samples of the dry composite coatings on the aluminum panels were shown in Figure 2.

Figure 2. The panel samples of each composite coating group

2.2.2 Glossiness evaluation

For evaluation of the gloss effects of the additives, glossmeter was chosen and the panels were studied for hardener effects on glossiness. In Figure 3, Novo Gloss trigloss device which was used in the study and is a gloss meter is shown.

Figure 3. Glossmeter

2.2.3 Pencil hardness

To determine the hardness of the surface from soft to hard as shown below, pencils with standard hardness must be used. The hardness level would be determined when the pencil leaves a permanent mark on the surface is defined as pencil hardness (ASTM D 3363). The apparatus of the pencil hardness measurement is given in Figure 4.

Figure 4. Pencil hardness

2.2.4 Universal impact tester

ASTM D 2794 provides a procedure for a rapid deform impact on a coating film and its substrate. If after the test some cracks were visible on the surface, then the test failed. In Figure 5, a universal impact tester (a) and a failed sample with cracks (b) have been shown.

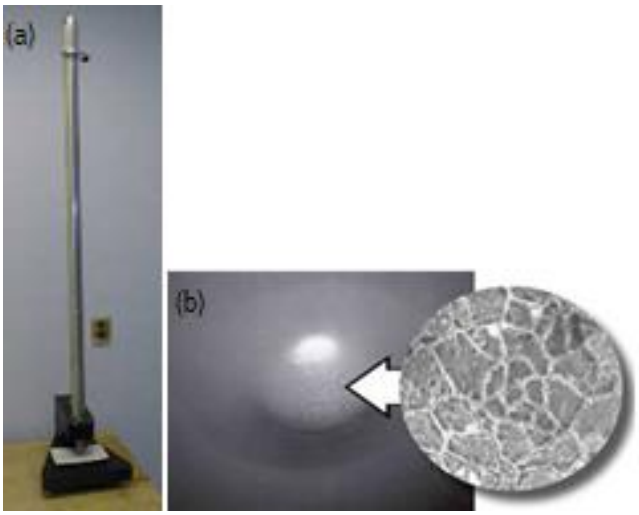

Figure 5. (a) A universal impact tester and, (b) a failed sample with cracks

2.2.5 Conical bent flexion

For evaluation of the flexibility of the samples with different hardeners, the conical bent flexion tester was chosen. It would be used to see if there are any positive or negative effects of the different additives. In Figure 6, a conical bent flexion apparatus is shown.

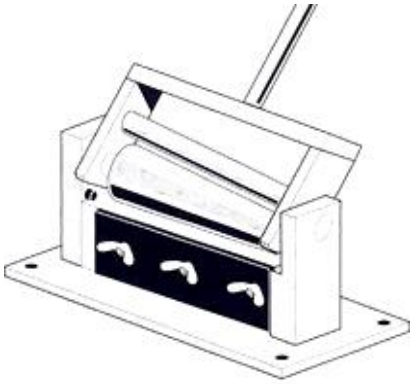

Figure 6. Conical bent flexion apparatus

2.2.6 Corrosion test (ISO 12944)

The corrosion test was done for all the five groups of the study. The method of ISO 12944 was followed in this appraisal. The samples were crossed over the middle and then placed in the corrosion cabinet. The preparation and placement of the panels in the corrosion cabinet have been shown in Figure 7.

Figure 7. Corrosion tests for the panels of the last session

"Corrosion tests in artificial atmospheres - Salt spray tests (TS EN ISO 9227)" was done on the samples. From each group, 3 repeated samples were examined. The samples were checked visually after 120 h, 240h, and 480h.

2.2.7 QCT test

The samples in 5 groups and 3 repeats were tested with a QCT test and observed after 120, 240 and 480h. Then cross-cut test was performed on the panels to see the potential effects of the humidity on the panels. In Figure 8, QCT test and the panels of the study were shown.

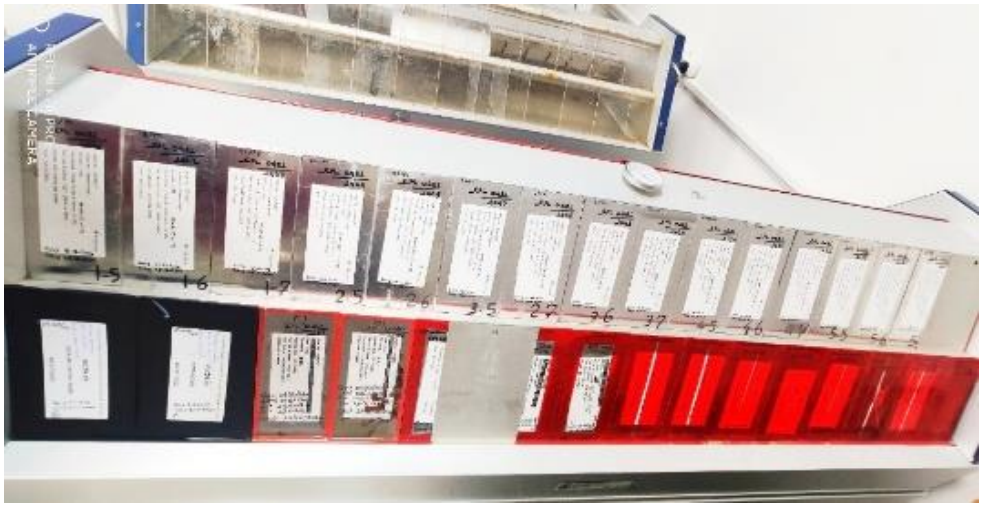

Figure 8. QCT test cabinet and the placed panels

The panels in the QCT test cabinet were placed fronted to the humidity to see the effects of the humidity on the coatings. After completion of 480h specimens were exposed to the cross-cut test.

2.2.8 Chemical resistance

Chemical resistance tests in this study were performed on the prepared panels. Chemical resistance tests included H_2SO_4 (10%) resistance test, NaOH (25%) resistance test and diesel resistance tests were carried out. In the following these tests have been explained in detail in order.

2.2.9 Sulfuric acid (10%)

H_2SO_4 (10%) test with immersion method was done on the panels. In this test a panel of any group was placed inside the H_2SO_4 solution. Immersing issue was done in a container which was shown in Figure 9. The samples were observed for 14 days.

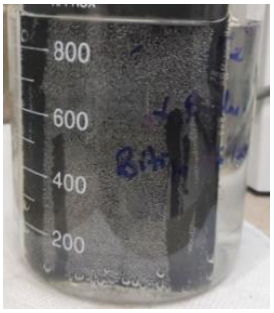

Figure 9. Resistance test against H_2SO_4 (10%) with immersion method

2.2.10 Sodium hydroxide (25%)

The chemical resistance tests were continued by with the scrubbing method which is shown in Figure 10.

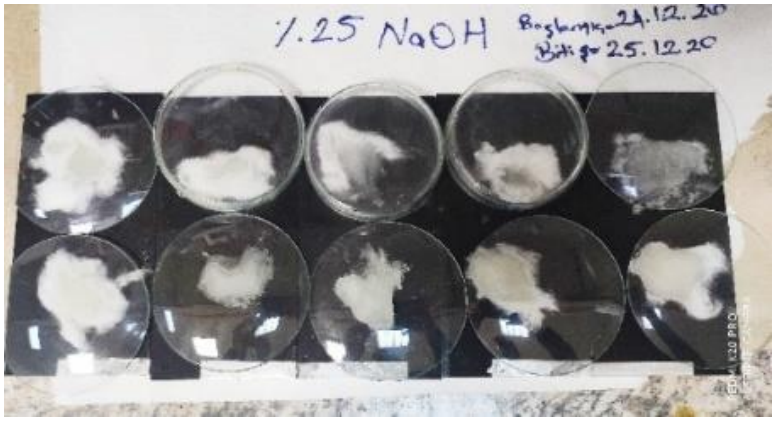

Figure 10. NaOH (25%) resistance test with the wetting method

2.2.11 Resistance against diesel

The tests of chemical resistance were continued by diesel resistance test. The method of diesel resistance test was similar to the NaOH resistance test. Saturated cotton pieces were placed upon the panels for 14 days. The panels were observed every day for 14 days.

3. Results and Discussion

At first, received sample has been analyzed to obtain a standard surface and thickness and to acquire further insights into their performance in glossiness, corrosion, QCT test, and chemical resistance tests. In this part, the results of all the tests have been given in order.

3.1 Glossiness Evaluation

The results of the glossmeter (in Table 2) upon the primers showed that addition of the additives negatively affected the gloss value of the surface and increased the opacity. The highest reduction happened in the samples containing B_4C. Reduction in glossiness of the coating samples containing hardening materials is inevitable as these materials are very small particles which embed inside of the resin molecules then these grains become exposed to the surface, scattering the light and providing matte effect. In the meanwhile, B_4C particles because of their amorphous shape and darker color influence the glossiness more.

Table 2. The results of the glossmeter of the surface of examination coatings

Gloss value	Blank	Black SiC	B_4C	Green SiC	Al_2O_3
(GU)	18.3	4.5	3.7	4.3	4.9

3.2 Pencil Hardness

The pencil hardness did not make big difference for the samples. All pieces failed on the H Pencil and only passed the F pencil. The surfaces were checked with a microscope for HB pencil test and there was no sign of scratch in the surface of the samples. The cases after the pencil hardness test are shown in Figure 11.

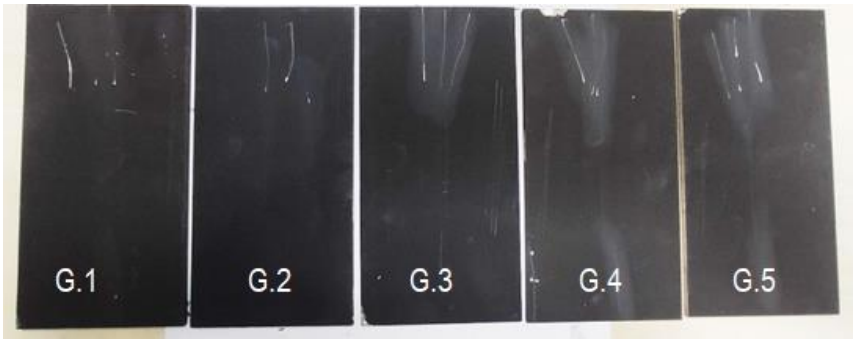

Figure 11. Results of the pencil hardness test

3.3 Universal Impact Tester

From the results of the impact tester, it could be considered that adding the hardeners did not affect negatively the flexibility and adhesion of the composite coating. The results were shown in Figure 12.

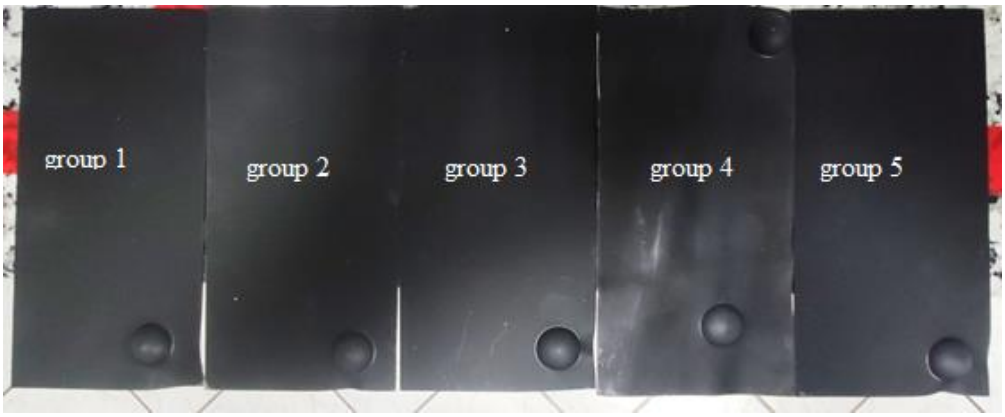

Figure 12. Results of the universal impact test

3.4 Conical Bent Flexion

The results of this test also showed no crack of peeling sign for the samples with or without the additives. This could be because of the high flexibility characteristics of the PTFE polymer structure which is the dominant resin in the primer and topcoat formulations. The results of the test were shown in Figure 13.

Figure 13. Results of the conical bent flexion test for the different groups of the study

3.5 Corrosion

After 120h the results did not show any sign of corrosion. In the time of 240h also the process didn't show significant corrosion sign but after 480h some white corrosion stains were observed. The results of the corrosion test after 480h were shown in Figure 14.

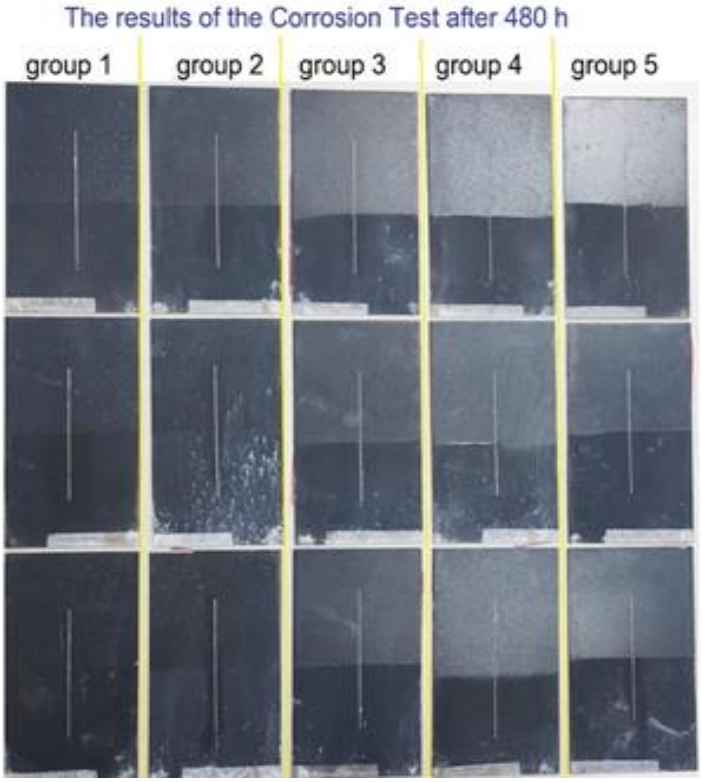

Figure 14. The panels of the 5 group after 480h corrosion test

The panels were analyzed according to TS EN ISO 4628-3 and ASTM D 714 standards. Corrosion test results, according to TS EN ISO 4628-3 and ASTM D 714 standards, are shown in Table 3.

Table 3. Corrosion test results based on TS EN ISO 4628-3 and ASTM D 714 standards

	Blank		Black SiC		B_4C		Green SiC		Al_2O_3	
	No8.	No8.	No8.	No8.	No8.	No8.	No8.	No8.	No6.	No6.
1	D	D	M	M	M	M	M	D	F	F
	Ri3	Ri0	Ri3	Ri0	Ri2	Ri0	Ri0	Ri0	Ri2	Ri0
	No6.	No6.	No8.	No8.	No8.	No8.	No8.	No8.	No6.	No6.
2	M	M	D	D	M	D	D	D	M	M
	Ri1	Ri0	Ri5	Ri2	Ri1	Ri0	Ri3	Ri0	Ri2	Ri0
	No8.	No8.	No8.	No8.	No8.	No8.	No8.	No8.	No6.	No6.
3	D	D	F	F	M	M	M	M	F	F
	Ri3	Ri0	Ri2	Ri0	Ri1	Ri0	Ri2	Ri0	Ri2	Ri0

3.6 QCT Test

The results showed no sign of blister or corrosion on the panels, and it indicates that humidity does not affect these coatings. Evaluation of the cross-cut tests also showed no difference between the fresh panels and the panels which exposed to QCT test. In Table 4, cross-cut test

results for fresh panels (left panel in every cell) and panels which exposed to QCT test (right panel in every cell) have been shown.

Table 4. Cross-cut test results for fresh panels (left panel in every cell) and panels which were exposed to QCT test (right panel in every cell)

	QCT test				
	Blank	**Black SiC**	**B_4C**	**Green SiC**	**Al_2O_3**
1	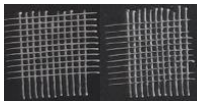		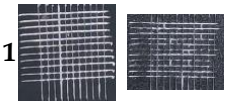	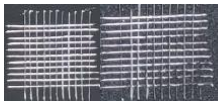	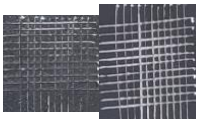
2	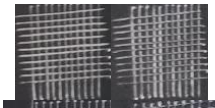	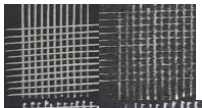	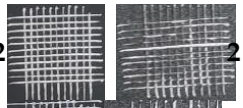	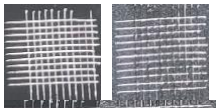	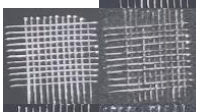
3	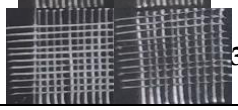	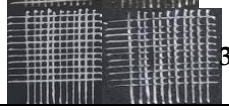	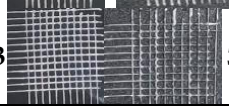	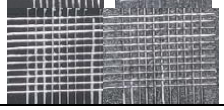	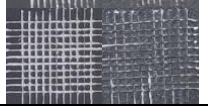

3.7 Chemical Resistance

At first days the surface resisted thoroughly against the acid solution but after 14 days the results showed some defects on most of the panels with primer coatings. The results are shown in Figure 15.

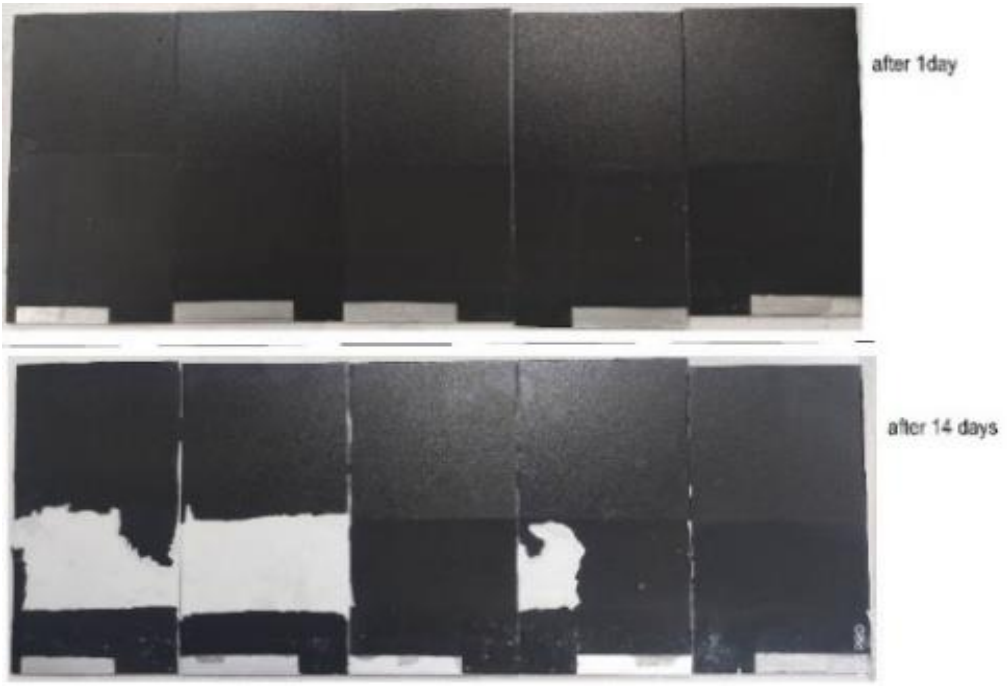

Figure 15. The results of the H_2SO_4 (10%) resistance test

In the case of NaOH (25%) resistance test, the panels were checked out after first days and also 14 days which can be seen in Figure 16.

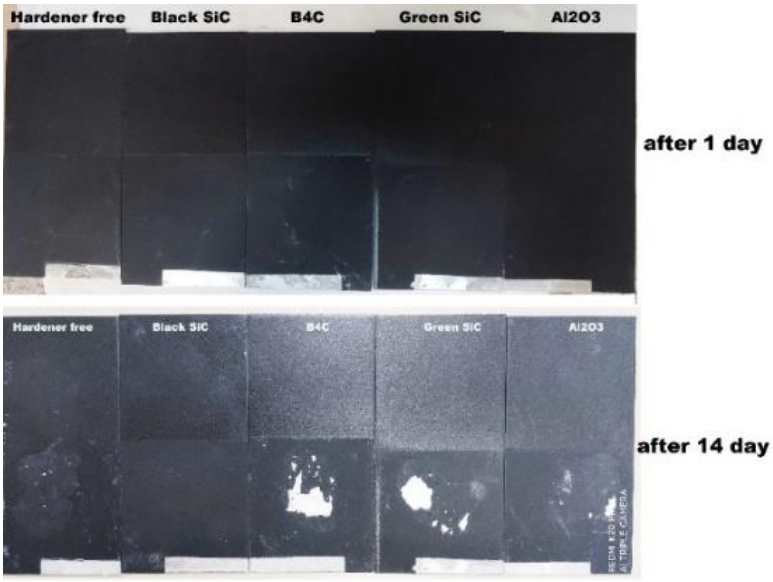

Figure 16. The results of the NaOH (25%) resistance test

These results showed no effect of the NaOH on topcoats of any groups but the last three groups have shown a sign of defection on their primer surfaces.

Diesel resistance examination of the coatings were accomplished and no sign of any defection was detected after this time. The resulted panels are shown in Figure 17.

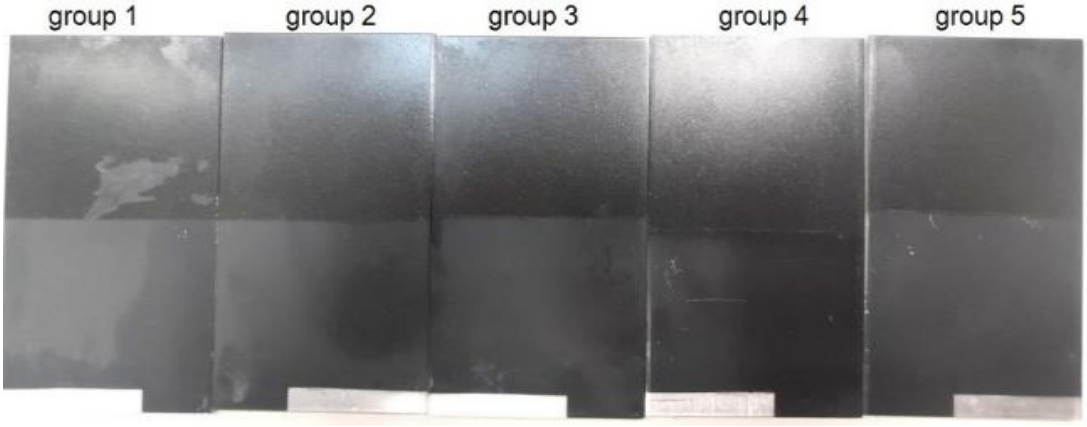

Figure 17. The results of the resistance test against diesel after 14 days

4. Conclusions

A non-stick surface is a surface engineered to reduce the ability of other materials to stick to it. Non-stick cookware is a common application, where the coatings allow food to brown without sticking to the pan. Most non-stick pans are coated with polytetrafluoroethylene.

In this study the effect of some additives known as hardening materials were studied in the subjects of glossiness, impact, hardness, conical bent, corrosion, humidity and chemical resistance. The results indicated that the samples containing B_4C were the best in overall performance following by black and green SiC . Although samples containing Al_2O_3 performed significantly better than samples lacking any hardener material, these samples were far behind the ones containing B_4C hardeners.

The samples with aluminum oxide was a head and shoulders behind these hard materials but samples including Al_2O_3 also was far better than the samples without any hardener material (blank sample). Glossiness of the samples containing hardener materials reduced when the additives were added to the coating formulation. Some other tests did not show significant difference among the samples.

Acknowledgments

The authors are grateful to THERNA brand which is a subsidiary of KANAT Paints and Coatings Company, Izmir, Turkey, for both the supply of the various coatings and test samples, and the financial support of this investigation. In addition, the help of THERNA research and development department technical experts in evaluation of the results is highly esteemed.

Author Statement

The authors confirm contribution to the paper as follows: study conception and design: Bikem ÖVEZ, Jabir ISMAEILI, Jigneshkumar PATEL; data collection: Jigneshkumar PATEL, Jabir ISMAEILI; analysis and interpretation of results: Bikem ÖVEZ, Jabir ISMAEILI; draft manuscript preparation: Jabir ISMAEILI. All authors reviewed the results and approved the final version of the manuscript.

Conflict of Interest

The authors declare no conflict of interest.

References

Abenojar J, Martínez M, Velasco F, Pascual-Sánchez V, Martín-Martínez J. (2009). Effect of boron carbide filler on the curing and mechanical properties of an epoxy resin. *The Journal of Adhesion*, 85(4-5), 216-238.

Beckford S, Cai J, Chen J, Zou M. (2014). Use of Au nanoparticle-filled PTFE films to produce low-friction and low-wear surface coatings. *Tribology Letters,* 56(2), 223-230.

Beckford S, Cai J, Fleming RA, Zou M. (2016). The effects of graphite filler on the tribological properties of polydopamine/PTFE coatings. *Tribology Letters,* 64(3), 42.

Chemours. New Teflon(TM) Profile Nonstick Coating 2017 [Available from: https://markets.businessinsider.com/news/stocks/new-teflon-tm-profile-nonstick-coating-combining-outstanding-nonstick-properties-with-long-term-scratch-resistance-1001935019.

Cheng X-H, Xue Y-J, Xie C-Y. (2002). Friction and wear of rare-earth modified glass-fiber filled PTFE composites in dry reciprocating sliding motion with impact loads. *Wear,* 253(7-8), 869-877.

Critchlow GW, Litchfield RE, Sutherland I, Grandy DB, Wilson S. (2006). A review and comparative study of release coatings for optimised abhesion in resin transfer moulding applications. *International Journal of Adhesion and Adhesives*, 26(8), 577-599.

Drobny JG. (2007). Fluoropolymers in automotive applications. *Polymers for Advanced Technologies*, 18(2), 117-121.

Drobny JG. (2020). *Applications of Fluoropolymer Films: Properties, Processing, and Products*: William Andrew.

Ebnesajjad S. (2015). *Fluoroplastics* (Vol 2): Melt processible fluoropolymers-the definitive user's guide and data book: William Andrew.

Ebnesajjad S, Morgan R. (2019). *Fluoropolymer Additives*: William Andrew.

Hatzikiriakos S. (2012). Rheology and processing of tetrafluoroethylene/hexafluoropropylene copolymers. *International Polymer Processing*, 27(2), 167-80.

Khedkar J, Negulescu I, Meletis EI. (2002). Sliding wear behavior of PTFE composites. *Wear*, 252(5-6), 361-369.

Kutelia E, Gventsadze D, Padgurskas J, Gventsadze L, Tsurtsumia O, editors. (2015). Investigation of the tribological properties of polytetrafluorethylene modified with metallic and nonmetallic nano particles, In: Proceedings of the BALTTRIB'2015: 8th international scientific conference dedicated to 50th anniversary year of Tribology, Aleksandras Stulginskis University, Kaunas, Lithuania.

Lee J-Y, Lim D-P, Lim D-S. (2007). Tribological behavior of PTFE nanocomposite films reinforced with carbon nanoparticles. *Composites Part B: Engineering*, 38(7-8), 810-816.

McKeen LW. (2019). *The Effect of UV Light and Weather on Plastics and Elastomers*: William Andrew.

Rossi S, Valdrè F, Calovi M. (2022). Validation of adhesion characterization methods for antistick coatings applied in cooking systems. *Journal of Coatings Technology and Research*.

Tevrüz T. (1998). Tribological behaviours of carbon filled polytetrafluoroethylene (PTFE) dry journal bearings. *Wear*, 221(1), 61-68.

Tevrüz T. (1999). Tribological behaviours of bronze-filled polytetrafluoroethylene dry journal bearings. *Wear*, 230(1), 61-69.

Thomas P. (1998). The use of fluoropolymers for non-stick cooking utensils. *Surface Coatings International*, 81(12), 604-609.

Yu C, Wan H, Chen L, Li H, Cui H, Ju P, et al. (2018). Marvelous abilities for polyhedral oligomeric silsesquioxane to improve tribological properties of polyamide-imide/polytetrafluoroethylene coatings. *Journal of Materials Science*, 53(17), 12616-12627.

Scientific Research Communications

Research Article

Sci. Res. Comm. (2022)
Volume 2, Issue 2
doi: 10.52460/src.2022.008

Application of the WASP Model for Assessment of Aeration Impact on Water Quality of Porsuk River, Turkey

Emre Dumlu[1,*] **Şebnem Elçi**[1]

[1] Civil Engineering Department, İzmir Institute of Technology, 35430 Urla/İzmir
[*] Corresponding author: emredumlu@iyte.edu.tr

Received: 15.08.2022 Accepted: 20.10.2022

Abstract

Porsuk Stream is the longest branch of the Sakarya Basin which originates from Murat Mountain and bypasses the provinces of Kutahya and Eskisehir. Based on recent increasing pollution concentrations reported in the literature, the main river is experiencing problems with decreased water quality. In this study, hydrodynamics and water quality parameters are simulated in the Porsuk River via the application of the Water Quality Analysis Simulation Program (WASP) using the available flow and meteorological data. After the validation of the hydrodynamics along the main river, water quality parameters are simulated using the eutrophication module. Simulation of dissolved oxygen concentrations pointed out hypoxia, especially at two locations; Kutahya-Reservoir1 and Alpu-Guroluk segments where dissolved oxygen values stayed well below the standard limits throughout the year. As a mitigation option, aeration applications at these two stations are proposed and the effects of aeration on the simulated parameters of dissolved oxygen, phosphorus and nitrate concentrations are investigated. Aeration at two segments has significantly improved the dissolved oxygen concentrations (from ~3 mg/l to >14 mg/l) whereas it has a more subtle effect on nitrate and phosphorus concentrations.

Keywords: WASP model, Porsuk River, water quality, aeration

1. Introduction

High nutrient concentrations and high turbidity often result in cyanobacterial blooms in water systems. Cyanobacterial blooms are likely to increase in frequency and intensity in response to climate change and eutrophication factors. The presence of cyanobacteria above 2000 cells/ml in potable water supplies can cause taste and odor problems, which increase the cost of water treatment. Higher levels of cyanobacteria (>50 000 cells/ml) render surface waters unsuitable for contact whereas very high levels, as occur in floating blooms, can result in fish kills and are potentially lethal when consumed (Hickey and Gibbs, 2009). Increases in toxins are all impacts of planktonic cyanobacterial blooms, whereas the bloom collapses may result in the creation of ammonia (Havens, 2008). It has been challenging to come up with complete explanations for why these species have thrived (Hyenstrand et al., 1998). A relationship has been found that cyanobacterial dominance (>50% of the phytoplankton population) increases rapidly when total P increases (Downing et al., 2001).

Freshwater systems are vital in supplying water for drinking, growing crops, manufacturing and energy and transport. Therefore, seasonal changes of water quality largely affect not only

the watershed area, but also ecosystem in region of interest. In recent years, excessive population growth, rapid increase in urbanization and industrialization, accompanied by the adverse effects of climate change, put increased pressure on the natural water resources and resulted in pollution of the existing resources that are already limited.

Water quality models are essential tools for effective management of water resources and play an important role in decision-making by providing water quality simulations and by allowing testing of a variety of management actions. Over the years, they have become an important tool for identifying water pollution and the final fate and behaviors of pollutants in a water environment (Wang et al., 2009). A wide range of models from simple to highly sophisticated numerical applications for simulating water quality has been developed. Burigato Costa et al. (2019) provided a review of the water quality models and stated that based on their review of the water quality-related studies conducted in the past 21 years water quality simulations: An aquatic ecosystem and toxicant simulation model (AQUATOX), two-dimensional hydrodynamic and water-quality model (CE-QUAL-W2), enviromental fluid dynamics code (EFDC), one-dimensional steady-state water quality models (QUALs), soil and water assessment tool (SWAT), spatially referenced regressions on watershed (SPARROW), and the water quality analysis simulation program (WASP) have been widely applied around the world. WASP, supported and developed by the US Environmental Protection Agency (USEPA), is a multi-dimensional and dynamic water quality modeling program. The model can be used to analyze a variety of water quality problems in ponds, streams, lakes, reservoirs, rivers, estuaries, and coastal waters. The time-varying processes of advection, dispersion, point and diffuse mass loading and boundary exchange are represented in the model.

The numerical model selected in this study, the water quality analysis simulation program (WASP); is a differential, spatially resolved, mass balance, fate and transport modeling framework structured to allow users to simulate concentrations of environmental contaminants in surface waters and bottom sediments (Ambrose et al., 1993). Water quality analyses are implemented for the water year of 2015 (10/1/2014 - 9/30/2015) using the WASP model. The Porsuk main river is divided into 25 segments in total, based on the available monitored water quality data. In Kose et. al, (2016), water quality parameters were collected from 18 stations located on the Porsuk Stream in 2015 and some important physicochemical parameters were investigated to determine the water quality of the stream. While dividing the main river into segments, segment length is set to 20 km at most, and the segments are named considering the starting and the ending locations. The average width and length of each segment are then calculated. For calibration of the model, all the available stations; Beskaris, Porsuk Ciftligi, Calca, Esenkara, Parsibey and Kiranharmani are considered, and the flow rates are obtained from The General Directorate of State Hydraulic Works (DSI) and The General Directorate of Electrical Power Resources Survey and Development Administration (EIE). Once the numerical model is calibrated based on flow rates, water quality parameters are simulated. Observed dissolved oxygen, phosphorus and nitrate concentrations are also implemented to validate the model. In the final part, aeration is proposed as mitigation for hypoxia observed at some stations and the effects of aeration on the simulated results are discussed.

2. Methodology

2.1. Study Site

Porsuk Stream Basin, a branch of the Sakarya river extends 201 km in the East-West direction in Northwest Anatolia and reaches 135 km of distance in the south direction and covers a precipitation area of 10,869 km² (Tekkanat and Sarış, 2015). It originates from Murat Mountain and flows into the Sakarya River after passing through Kutahya and Eskisehir provinces. The

study area, segmentation of the river and available stations along the river are given in Figure 1 (Dumlu and Elçi, 2022). In Figure 1, stations where water quality parameters were monitored by Köse et al. (2016), are presented with blue dots, stations where flow data are monitored by DSI are marked with brown dots. Additional stations added for the segmentation are shown by green dots. The reference coordinate system is arranged to WGS 84/Pseudo-Mercator (EPSG:3857).

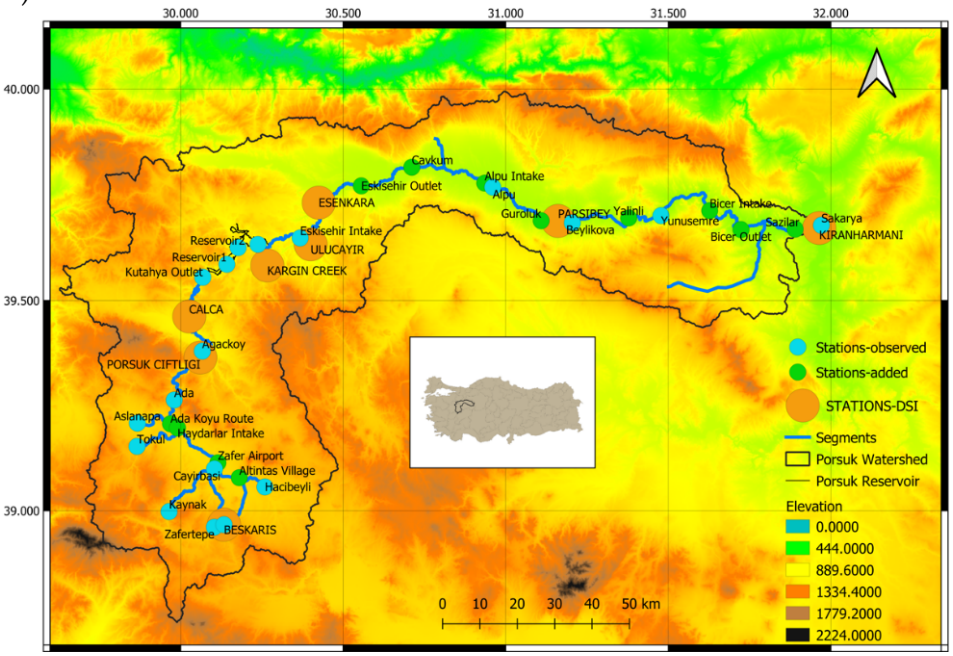

Figure 1: Porsuk watershed and locations of stations considered in the model

2.2 Data Sources

The meteorological data are downloaded from Giovanni for the nearest stations: Alpu and Zafer Airport. 'Giovanni', an open data portal of NASA between 10/1/2014-09/30/2015 (https://giovanni.gsfc.nasa.gov/giovanni, accessed on 25th July 2022). The Goddard Earth Sciences Data and Information Services Center (GES DISC) has created web-based GES DISC Interactive Online Visualization and Analysis Infrastructure, (Giovanni), to enable analysis of satellite remotely sensed meteorological, oceanographic, and hydrologic data sets. The AIRS3STD model is used for the air temperature in the availability of data bounding box 30.5E, 39.59N, while the GLDAS model was used for the available data bounding box 29.875N, 39.625E for both wind speed and solar radiation time series, respectively.

The flow rate data at Beskaris, Porsuk Ciftligi, Calca, Esenkara, Parsibey, and Kiranharmani stations are obtained from the State Hydraulic Works for the water year of 2015.

The observed air temperature, wind speed and solar radiation data for the water year of 2015 are presented in Figures 2,3 and 4.

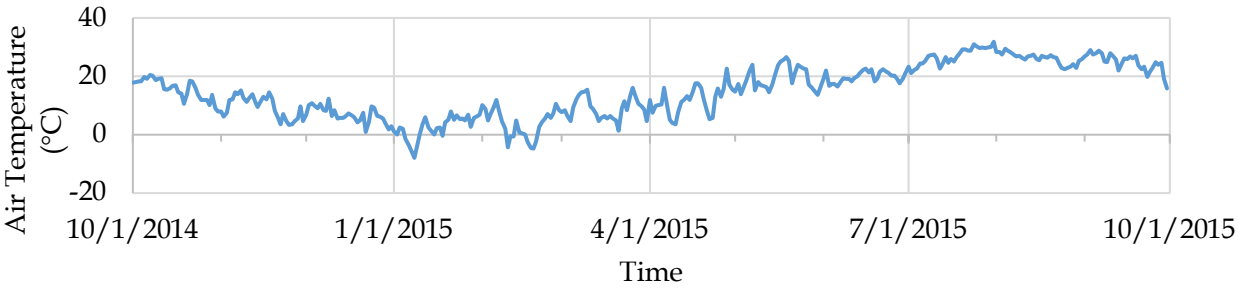

Figure 2: Monitored air temperatures

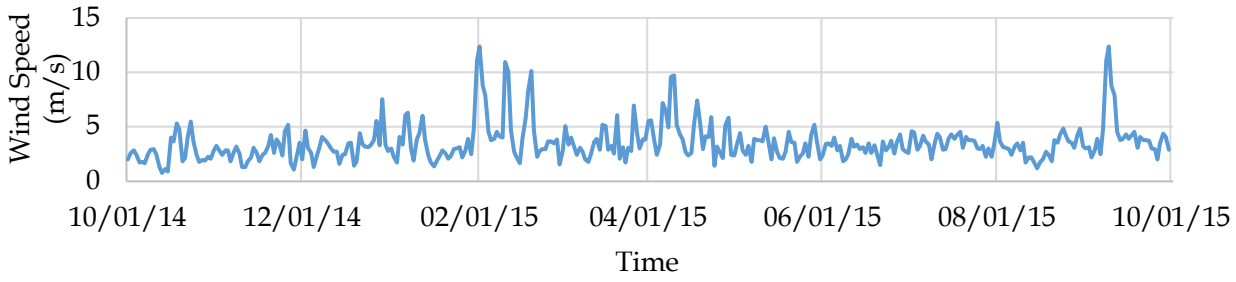

Figure 3: Monitored wind speed data

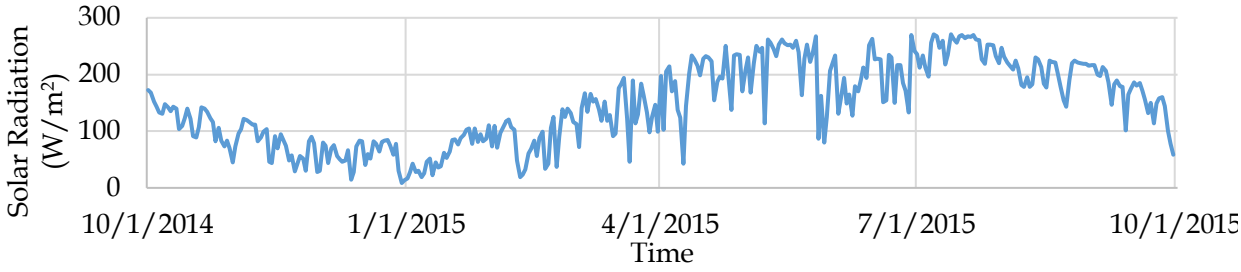

Figure 4: Monitored solar radiation data

The validity of the data (Giovanni) is tested by comparing the data monitored at the two meteorological stations close to the study site. Daily air temperatures from ALPU and Zafer Airport stations are obtained and averaged and then compared with the data downloaded from Giovanni for our study region (Figure 5). Results indicated that the data from Giovanni overpredicted the monitored data but the correlation between two data sets was high having R^2 of 0.90.

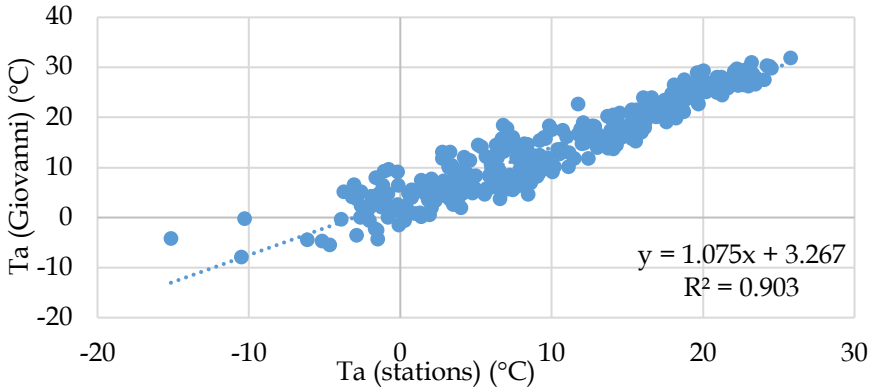

Figure 5. Comparison of monitored air temperatures with the data downloaded from Giovanni

Next, we obtained the monitored water temperature data for Besdegirmen station located in the study site from the State Hydraulic Works. Water temperature data was available for seven years (2006-2013) and collected once a month. For the specific dates when the monitoring took place, daily water temperatures are derived from the monitored daily air temperatures for the stations. Water temperatures monitored once a month at the suspended sediment monitoring station of Besdegirmen are obtained between 2006-2012 and are used to issue a relation between the measured water temperatures and the air temperatures for the corresponding

dates of the measurements. The equation relating air temperatures to water temperatures is derived as in Eq (1):

$$T_w = 0.487 * T_a + 8.6027 \quad (1)$$

where T_w is the water temperature (°C) while, T_a is the air temperature (°C).

Next, we compared water temperatures predicted by the air temperature data from the monitoring stations and Giovanni with the monitored water temperatures (Figure 6). Results showed that the later comparison had a better correlation with the monitored water temperature data. This analysis showed that meteorological data downloaded from Giovanni can be used for predicting water temperature in the streams and are well correlated with the monitored meteorological data at the study site (Figure 7).

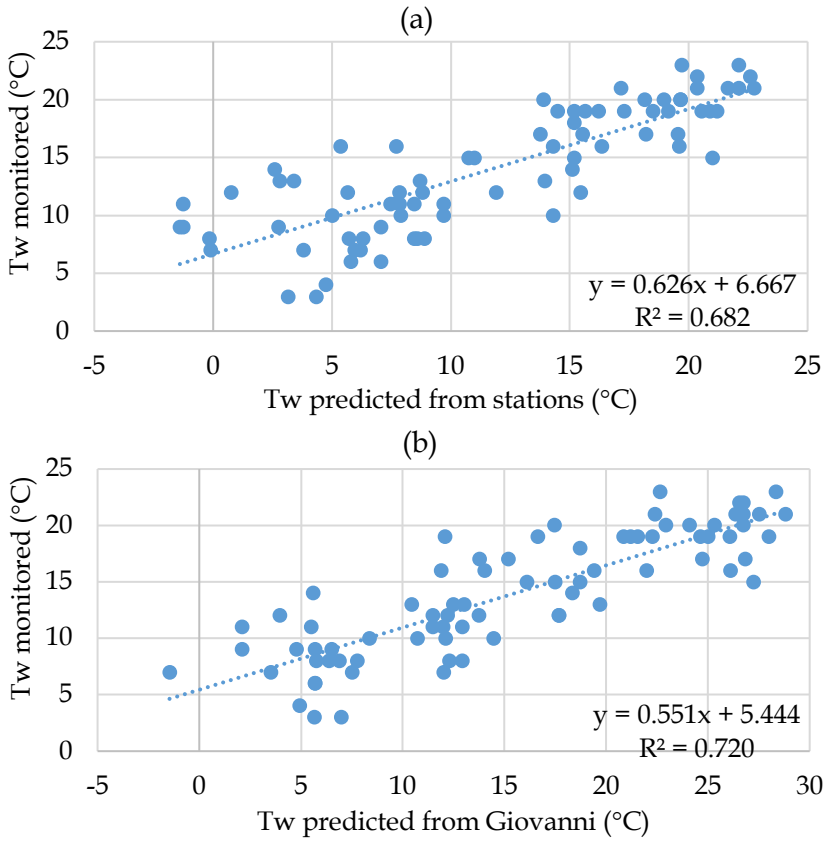

Figure 6. (a) Comparison of predicted water temperatures by the air temperature data from the monitoring stations with the monitored water temperatures, (b) Comparison of predicted water temperatures by the data from Giovanni with the monitored water temperatures

Eq. (1) is then used to find the values of daily water temperature data to be used as input to the model for the water year of 2015. The data presented in Figure 8 are used as water temperature time series input to the model for the simulation period.

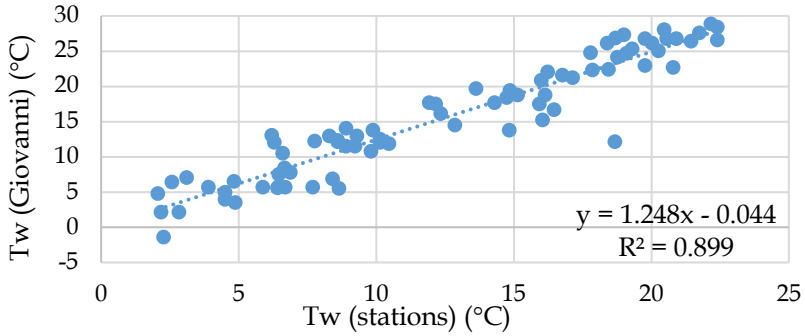

Figure 7. Comparison of water temperatures predicted using the air temperature data from the monitoring stations with the water temperatures predicted using the air temperature data from Giovanni

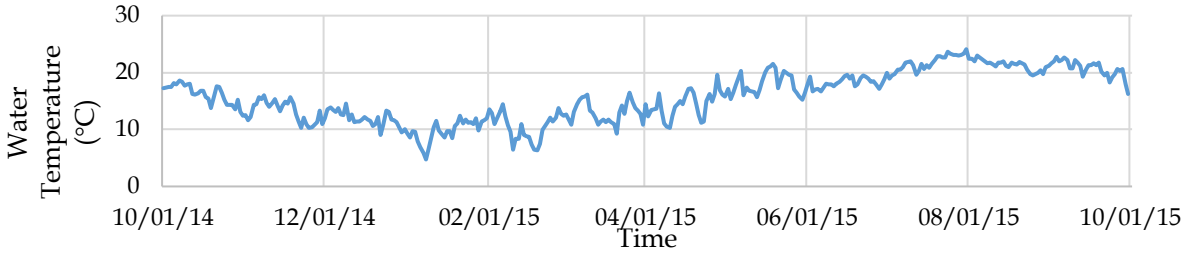

Figure 8. Water Temperature Time Series used in the simulations

2.3. Application of the WASP Model

WASP also can be linked with hydrodynamic and sediment transport models that can provide flows, depths, velocities, temperature, salinity and sediment fluxes. WASP contains four layers representing different parts of water ecosystems. These layers are defined as 1) The water column in contact with the atmosphere, 2) The water column non-contact with the atmosphere, 3) The underlying benthos in contact with water, 4) The sediment bed non-contact with water. When the conservation of mass and momentum are solved for both water and solids between the layers, flow and transport in the water column, transport in the porous media of the bed sediment, transport in the water column via settling/re-suspension and transport with rainfall/evaporation are considered. Although the model cannot execute hydrologic computations, it can be linked to hydrologic models such as HSPF and SWIMM and can be linked to hydrodynamic models through input files. When WASP is used alone, it solves the hydrodynamics using the kinematic wave equation. It can also transfer data to the central database system developed by the EPA (Ambrose et al., 1993).

Water quality processes are represented in special kinetic subroutines that are either chosen from a library or written by the user. WASP is structured to permit easy substitution of kinetic subroutines into the overall package to form problem-specific models. WASP8 comes with four modules: TOXI for simulation of toxicants and EUTRO for simulation of conventional water quality, including ammonia, nitrate, dissolved oxygen, salinity, organic/inorganic phosphorus, MERCURY for simulation of mercury and HEAT for simulation of temperatures in water bodies.

WASP has been applied to various surface water systems, addressing a range of environmental contaminants. Recently, Shabani et al. (2021) simulated flood-induced soil, sediment, and contaminant transport by using a coupled hydrodynamic (HEC-RAS 2D) and water quality model (WASP). Wool et al. (2020) summarized the evolution of the model over the years. Some applications of WASP include : nutrient loading on water quality in Tampa Bay, Florida (Wang et al., 1999); mercury fate and transport in the Carson River, Nevada

(Carroll et al., 2000); impacts of climate change on water quality of Chungju Lake (South Korea) (Park et al., 2013); and the effects of increasing temperature and solar radiation due to climate change on water quality of the Sitalakhya River (Bangladesh) for the years 2009, 2030, 2050 and 2070 (Alam et al., 2013); the effects of air quality policy changes on water quality (Burian et al., 2022); the effects of farmland withdrawal water on the water quality (dissolved oxygen in the Danshui and Chungkang Rivers, Taiwan (Chen et al., 2012); algal dynamics in an urban river in Beijing (Jia et al., 2010); dissolved oxygen depletion in diverted floodwaters of the Elbe River, Germany (Lindenschmidt et al., 2009); eutrophication control in the Keban Dam Reservoir, Turkey (Soyupak et al., 1996); eutrophication control in El Pañe Reservoir (Larico et. al, 2019). Elçi et al. (2010), applied the WASP model to investigate the effects of Kizildere Geothermal Power Plant discharges on the water quality of the B. Menderes River. Kannel and Gan (2013), applied the WASP model to investigate the potential impacts of oil sand processed water in terms of water quality by dividing the Athabasca River water body into 46 rectangular segments. The model was also applied to simulate various copper effluent control measures and impacts of the heavy rainfall by the climate change on copper concentrations by dividing the mainstream of Erren River into 189 segments (Chueh et. al, 2021). Obin et al. (2021) implemented the model to simulate the water quality concentrations such as; chemical oxygen demand (COD), ammonium nitrogen (AN) and total phosphorus (TP) and predict the water environmental capacity in Lushui River, China. Seo et al. (2012), predicted chlorophyll-a changes due to weir constructions by dividing the Nakong river, South Korea into eleven reaching. Iqbal et al. (2018) investigated the effects of the physical geometry of wastewater-treatment facilities on pollution concentrations in Ravi River (Pakistan) by dividing the river into eighteen segments.

In this study, for the application of the WASP model to predict water quality parameters, Porsuk river is divided into 25 segments and location and physical properties of each segment are defined respectively in Table 1.

Table 1. Location and physical properties of the main river segments used in the model

Segment No	X coordinate	Y coordinate	Segment Name	Length (m)	Width (m)	Slope (θ)
2	39.07876	30.1808	Altintas Village- Zafer Airport	8569.3	6.9	0.00082
3	39.11447	30.11463	Zafer Airport-Haydarlar Intake	15405.5	25.7	0.00045
4	39.19748	29.99047	Haydarlar-Adakoyu Route	3091.5	14.8	0.00032
5	39.20738	29.9687	Adakoyu Route-Ada	7647.4	13.7	0.00026
6	39.26397	29.98031	Ada-Agackoy	20000.0	15.2	0.00260
7	39.38014	30.06653	Agackoy- Calca	20000	22.95	0.00105
8	39.46242	30.02649	Calca-Kutahya Intake	15210.4	24.8	0.00092
9	39.55533	30.06802	Kutahya Outlet-Reservoir1	12468.5	77.3	0.00128
10	39.586	30.14198	Reservoir1-Reservoir2	6046	1363.2	0
11	39.62566	30.17688	Reservoir2-Reservoir3	5845.7	1724.1	0
12	39.63312	30.23757	Reservoir3-Eskisehir Intake	20000	54	0.0026
13	39.64833	30.36753	Eskisehir Intake-Esenkara	20000	21.42	0.0012
14	39.72944	30.4248	Esenkara-Eskisehir Outlet	20000	23.78	0.0012
15	39.77156	30.55555	Eskisehir Outlet-Cavkum	20000	24.5	0.0006
16	39.81572	30.71093	Cavkum-Alpu Intake	20000	18.7	0.0005
17	39.77813	30.93529	Alpu Intake-Alpu	2693.8	18.4	0.00037
18	39.76836	30.96016	Alpu-Guroluk	20000	20.1	0.00015
19	39.68892	31.10943	Guroluk-Beylikova	12229.3	15.3	0.00049
20	39.68423	31.20469	Beylikova-Yalinli	20000	22.4	0.00055
21	39.69572	31.37774	Yalinli-Yunusemre	12404.1	18.9	0.00048
22	39.70131	31.47751	Yunusemre-Bicer Intake	20000	17.4	0.0009
23	39.71313	31.62732	Bicer Intake-Outlet	20000	13.1	0.0011
24	39.66823	31.72424	Bicer Outlet-Sazilar	20000	12.7	0.00075
25	39.67838	31.9709	Sazilar-Sakarya	2370.1	13.4	0.00338

The river segmentation is performed based on monitoring stations where water quality data are available in the literature (Köse et al., 2016) and at the stations where flow rates are monitored regularly (Figure 1). Prior to the simulation of water quality parameters, simulation results of the hydrodynamics along the river are validated with the available observations. For these simulations, the eutrophication module (EUTRO) is selected, and 1-D kinematic wave approach is utilized. The maximum time step is set to 2.46 minutes in the simulations. The flow rates are output at all stations daily for the simulation period (10/1/2014-9/30/2015). For the model domain, the segments are specified as input based on the properties summarized in Table 1. The parameters measured at the stations at the beginning of the simulation period are specified in the model as initial conditions. The daily values of air temperature, wind speed, solar radiation, and water temperature are provided as input data for the simulation period.

The model is calibrated using the following parameters (Table 2) based on the literature (Larico and Medina, 2019).

Table 2. Kinetic constants for WASP model calibration (Larico and Medina, 2019).

Parameters	Calibrated Value
Global Constant	
Fresh water = 0 - Marine Water = 1	0
Ks Option	1
Salinity Simulation Option (1 = Salinity- 2 = TDS)	1
Water Temperature	
Heat exchange option (0=full heat balance- 1=equilibrium temperature)	0
Sediment (ground) temperature- °C	10
Ice switch (0 = no ice solution- 1=ice solution- 2=detailed ice solution)	0
Inorganic Nutrient Kinetics	
Nitrification Rate Constant at 20 degree C (1/day)	0.425
Nitrification Temperature Coefficient	1
Half Saturation Constant for Nitrification Oxygen Limit (mg O2/L)	1.00E-06
Minimum Temperature for Nitrification Reaction (degree C)	7
Denitrification Rate Constant at 20 degree C (1/day)	0.01
Denitrification Temperature Coefficient	1
Half Saturation Constant for Denitrification Oxygen Limit (mg O2/L)	1.00E-06
Organic Nutrients	
Dissolved Organic Phosphorus Mineralization Rate Constant at 20 C (1/day)	0
Dissolved Organic Phosphorus Mineralization Temperature Coefficient	1
Dissolved Oxygen	
Global Reaeration Rate Constant at 20 C (1/day)	5
Oxygen to Carbon Stoichiometric Ratio	2.667
Theta -- Reaeration Temperature Correction	1.024
Theta -- SOD Temperature Correction	1.04

After calibration of the kinematic constants, the comparison of simulated water temperatures and observed water temperatures which were obtained from Kose et. al, 2016, are given in Table 3.

Table 3. Comparison of simulated and observed water temperature values

Segment No	Segment Name	Simulated Water Temperature (July) (°C)	Observed Water Temperature (°C)
1	Beskaris-Altintas Village	17.9	18.1
6	Ada-Agackoy	23.0	22.8
7	Agackoy-Calca	22.2	22
9	Kutahya outlet-Reservoir 1	23.8	24
10	Reservoir 1- Reservoir 2	24.1	23.9
11	Reservoir 2- Reservoir 3	23.6	23.5
12	Reservoir 3- Eskisehir Intake	23.7	23.9
13	Eskisehir Intake-Esenkara	14.6	14.5
18	Alpu Outlet-Guroluk	21.1	21.3
20	Beylikova-Yalinli	23.4	23.4
22	Yunusemre-Bicer Intake	25.3	25.4
25	Sazilar-Sakarya	24.9	25

The RMSE and MAE values for the comparison are calculated as 0.13 °C (0.6% of the average temperature), and 0.15 °C (0.6% of the average temperature), respectively.

3. Results

3.1 Simulation of the Hydrodynamics

At inflow section, the flow functions showing flow time series at the boundaries of the model are specified using daily flow measurements recorded at the river monitoring stations. As shown previously in Figure 1, eight different flow functions are defined. Figure 9 presents the comparison of simulated flow rates with the observations for six different stations: Beskaris, Porsuk Ciftligi, Calca, Esenkara, Parsibey and Kiranharmani stations.

Error analysis is conducted to evaluate the errors between the predicted and observed discharge time series. The Root Mean Square Error (RMSE) and Mean Absolute Error (MAE) used to examine the difference between the observed and measured discharge time series are given as in Eq. (2) and Eq. (3):

$$RMSE = \sqrt{\sum_{i=1}^{n} \frac{\left(Q_{observed} - Q_{predicted}\right)^2}{n}} \quad (2)$$

$$MAE = \frac{1}{n}\sum_{i=1}^{n} \left| Q_{observed} - Q_{predicted} \right| \quad (3)$$

where *RMSE* is root mean square error, while *MAE* is mean absolute error. The calculated RMSE and MAE values for each station are given in Table 4.

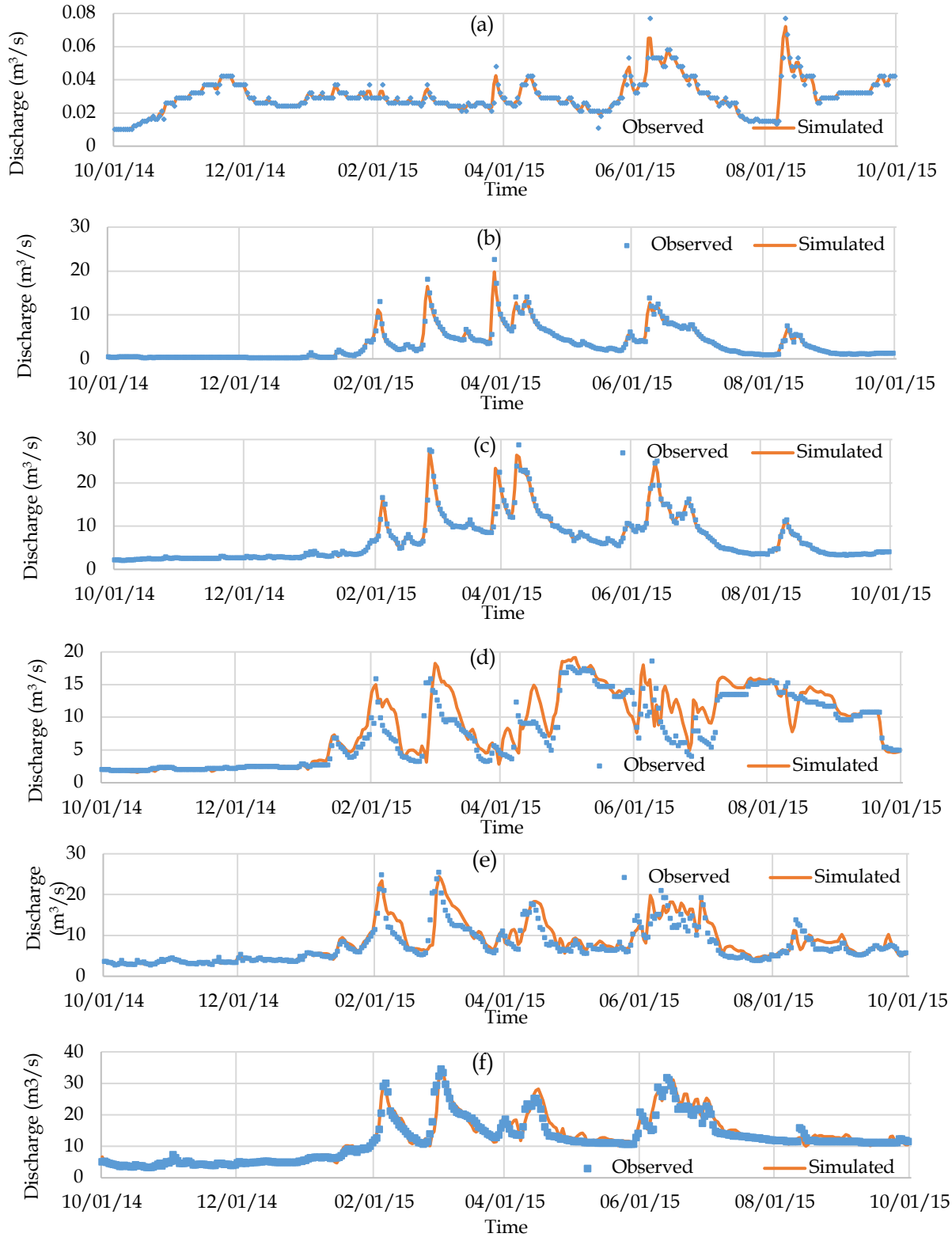

Figure 9. Comparison of flow rates at six stations;; a) Beskaris, b) Porsuk Ciftligi, c) Calca, d) Esenkara, e) Parsibey, f) Kiranharmani stations

Compared to the stations upstream of the river, higher RMSE values are calculated for Esenkara and Parsibey stations: 2.415 m^3/s (13% of the maximum discharge), and 2.088 m^3/s (8.2% of the maximum discharge), respectively (Table 3).

Table 4. RMSE and MAE values for discharge stations

Stations	Root Mean Square Error (RMSE)	Mean Absolute Error (MAE)
Beskaris	0.002	0.001
Porsuk Ciftligi	0.718	0.260
Calca	0.918	0.313
Esenkara	2.415	1.555
Parsibey	2.088	1.324
Kiranharmani	1.823	1.172

Next, we compared the simulated water temperatures with the observed ones (Figure 10). The RMSE and MAE values are calculated as 2.57˚C (11% of the maximum temperature) and 1.89 ˚C (8% of the maximum temperature), indicating that water temperatures are predicted reasonably for the purposes of the study.

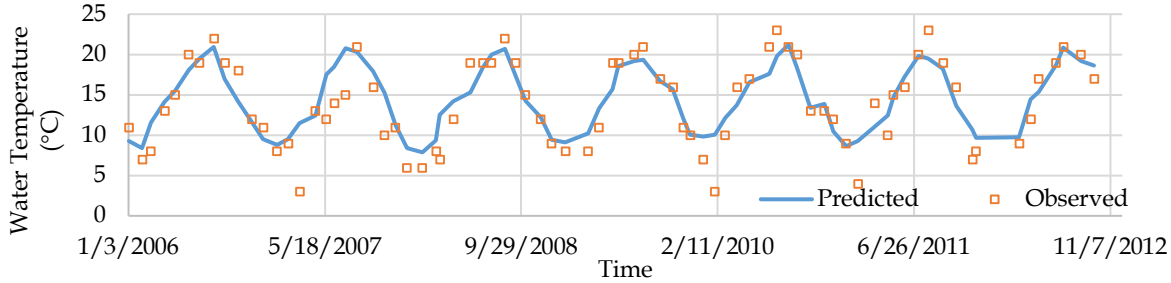

Figure 10. Comparison of observed water temperatures at Besdegirmen station with the simulated values predicted.

3.2 Simulation of the Water Quality Parameters

Following the simulation of discharges at monitoring stations accurately, water quality parameters are modeled. In the loads section, water quality parameters are specified as input data for the model segments according to sampling locations. The model is run for the water year of 2015 by the eutrophication module and the simulated dissolved oxygen concentrations, phosphorus and nitrate concentrations are compared with the observed values reported by Köse et al., (2016) (Table 5, 6 and 7). The simulated results are also presented along the river (Figure 11).

Table 5. Comparison of simulated and observed dissolved oxygen concentrations

Segment No	Segment Name	Simulated DO (mg/L)	Observed DO (mg/L)
1	Beskaris-Altintas Village	7.89	7.86
6	Ada-Agackoy	7.95	7.97
7	Agackoy-Calca	7.47	7.56
9	Kütahya outlet-Reservoir 1	3.33	3.3
10	Reservoir 1- Reservoir 2	14.19	14.14
11	Reservoir 2- Reservoir 3	13.32	13.24
12	Reservoir 3- Eskisehir Intake	13.83	13.8
13	Eskisehir Intake-Esenkara	7.99	7.92
18	Alpu Outlet-Guroluk	4.36	4.33
20	Beylikova-Yalinli	6.59	6.61
22	Yunusemre-Bicer Intake	5.62	5.66
25	Sazilar-Sakarya	7.93	7.97

Table 6. Comparison of simulated and observed phosphorus concentrations

Segment No	Segment Name	Simulated P (mg/L)	Observed P (mg/L)
1	Beskaris-Altintas Village	0.026	0.027
6	Ada-Agackoy	0.044	0.046
7	Agackoy-Calca	0.033	0.032
9	Kütahya outlet-Reservoir 1	0.293	0.307
10	Reservoir 1- Reservoir 2	0.076	0.074
11	Reservoir 2- Reservoir 3	0.059	0.054
12	Reservoir 3- Eskisehir Intake	0.028	0.026
13	Eskisehir Intake-Esenkara	0.314	0.307
18	Alpu Outlet-Guroluk	0.506	0.503
20	Beylikova-Yalinli	0.486	0.478
22	Yunusemre-Bicer Intake	0.504	0.498
25″	Sazilar-Sakarya	0.55	0.53

Table 7. Comparison of simulated and observed nitrate concentrations

Segment No	Segment Name	Simulated Nitrate (mg/L)	Observed Nitrate (mg/L)
1	Beskaris-Altintas Village	0.990	1.05
6	Ada-Agackoy	0.604	0.609
7	Agackoy-Calca	1.000	1.01
9	Kütahya outlet-Reservoir 1	0.903	0.91
10	Reservoir 1- Reservoir 2	0.152	0.158
11	Reservoir 2- Reservoir 3	0.342	0.342
12	Reservoir 3- Eskisehir Intake	0.232	0.228
13	Eskisehir Intake-Esenkara	0.638	0.631
18	Alpu Outlet-Guroluk	2.76	2.76
20	Beylikova-Yalinli	3.23	3.25
22	Yunusemre-Bicer Intake	3.39	3.38
25	Sazilar-Sakarya	2.92	2.98

The RMSE values for the comparison are calculated as 0.11 mg/L (1.3% of the average concentration) for the dissolved oxygen, 0.04 mg/L (16.8% of the average concentration) for phosphorus, 0.058 mg/L (4% of the average concentration) for nitrate.

Following this analysis, simulation results are also compared for two times of the year having very different flow regimes. Monthly averaged July and January concentrations are selected for this purpose. These periods are selected since the rivers is expected to have the lowest (July) and the highest (January) dissolved oxygen concentrations during these times of the year. Table 5 shows the concentrations predicted at different segments along the stream. Comparison of the simulation results indicated that in both months, lowest dissolved oxygen values are observed at specific locations: Kutahya-Reservoir1 segment 3.33 mg/L (Red dot), and at Alpu-Guroluk segment as 4.36 mg/L. At these stations simulated and observed dissolved oxygen values were below 5 mg/L throughout the year.

Next, the total phosphorus and nitrate concentrations along the stream for the two months: January and July were simulated. A significant increase in the observed/simulated total phosphorus is observed from 0 to 0,3 mg/l at the Kutahya-Reservoir1 segment and from 0,3 mg/L to 0,5 mg/l at the Alpu-Guroluk segment. As for the nitrate concentrations, a significant increase is observed from 0,63 mg/L to 2.76 mg/l at the Alpu-Guroluk segment.

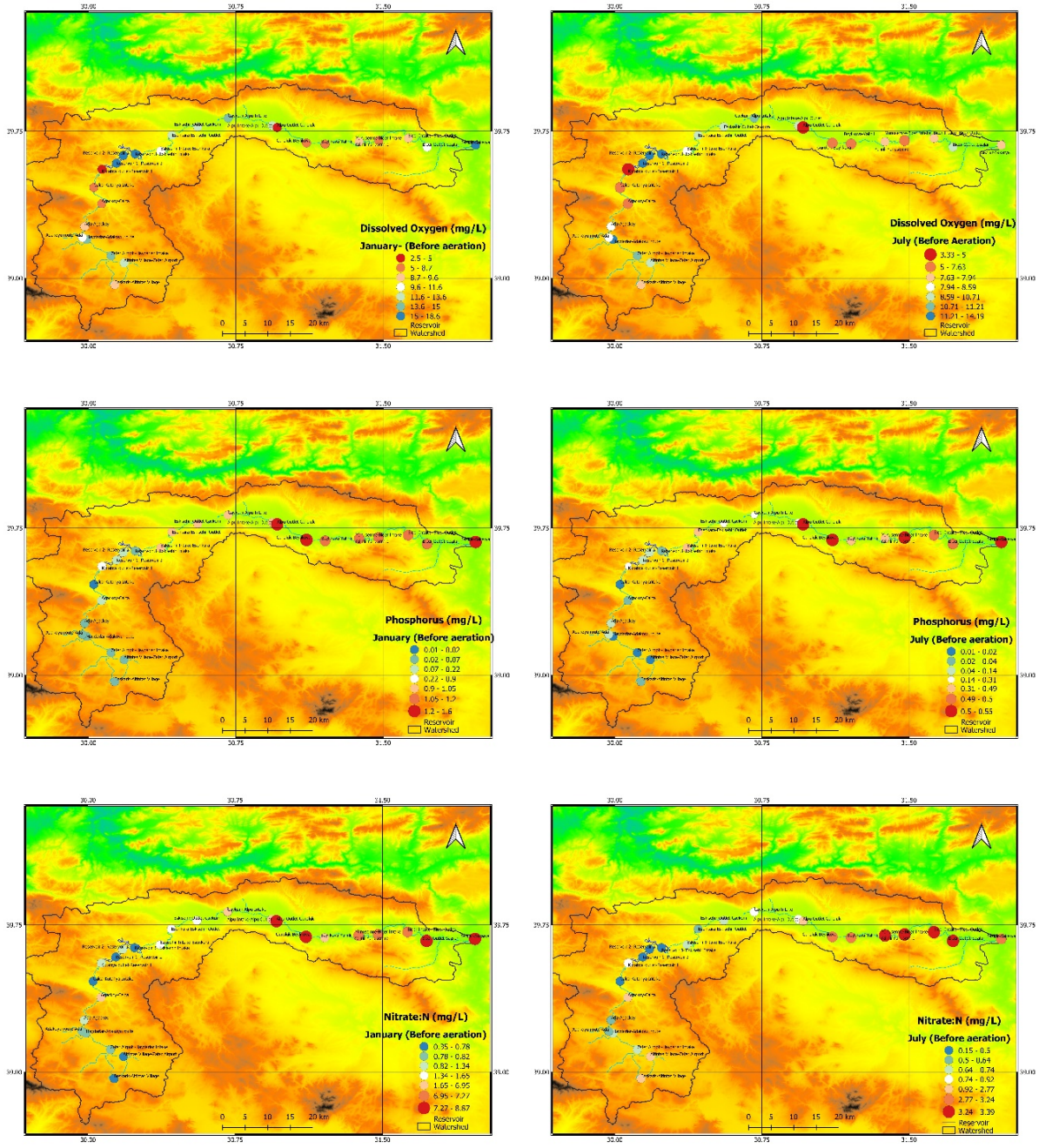

(a) (b)

Figure 11. Comparison of the simulated dissolved oxygen, phosphorus, and nitrate concentrations along the river for two different months; a) January, b) July

3.3 Proposed mitigation solution for the improvement of the water quality: Aeration

Aeration/oxygenation has been widely used to improve water quality associated with eutrophic conditions in water systems. In general, it is regarded as a good solution to prevent blooms of cyanobacteria because it reduces light availability (Beutel and Horne 1999).Various forms of hypolimnetic aeration/oxygenation systems have been installed to the lakes/reservoirs with varying degrees of success in the past (Holland and Tate, 1984; Gallagher, 1984; Meyer et al., 1992; Burns and Powling, 1981; Croome, 1981; Chipofya and Matapa, 2003; Horne, 2019; Horne and Beutel, 2019). A successful application of a hypolimnetic oxygenation system was utilized in a hatchery on the Mokelumne River,

California, following the death of 300,000 salmonid hatchery fish, suspectively by Hydrogen sulfide (H2S). Following the oxygenation operation, Chinook salmon returns rose significantly (Horne, 2019). In another application, long-term improvement in water quality was achieved by a hypolimnetic oxygenation system in Camanche Reservoir, California, a eutrophic reservoir, experiencing blooms of cyanobacteria. Within days of the application, water quality improved and hypolimnion phosphate and ammonium concentrations declined as stated in Horne and Beutel (2019). The previous design of artificial destratification systems was based on trial and error in the site, where neither the effect of air bubble size nor the effect of air density in the bubble plume could be investigated.

Following the successful applications in the literature, installations of aeration systems to two segments observed to have the lowest dissolved oxygen concentrations have been proposed in this study. The first aeration point is selected "Kütahya outlet-Reservoir1" segment (#9) to increase the dissolved oxygen concentrations to the maximum concentration value (14.2 mg/L) and to examine the effects of this change on the following segments. The simulated dissolved oxygen concentrations at the segments along the river, after the first aeration applied at "Kutahya outlet-Reservoir1" segment is given in Table 8. Based on the simulated results it was observed that beginning with the "Alpu Outlet-Guroluk" segment (#18) dissolved oxygen concentrations experience a sharp decrease and fall below 5 mg/L indicating of decreased water quality at the stretch of the river. Therefore, a second aeration is applied at this segment. Table 9 presents the results of the proposed aeration applied at two segments and gives a comparison of the simulated dissolved oxygen, phosphorus and nitrate concentrations for summer (July) and winter (January) before and after the application of the aeration. The simulated results are also presented along the river (Figure 12). As can be seen in Table 9, aeration at two segments has significantly improved the dissolved oxygen concentrations, whereas it has a more subtle effect on nitrate and phosphorus concentrations.

Table 8. The first aeration effects on the following segments

Segment No	Segment Name	Simulated DO-July (mg/L)	Simulated DO-January (mg/L)
1	Beskaris-Altintas Village	7.89	9.42
2	Altintas Village-Zafer Airport	10.71	13.59
3	Zafer Airport -Haydarlar Intake	11.20	14.53
4	Haydarlar-Adakoyu route	11.21	14.56
5	Adakoyu route-Ada	8.09	9.80
6	Ada-Agackoy	7.95	9.54
7	Agackoy-Calca	7.47	7.82
8	Calca-Kutahya Intake	5.94	6.18
9	Kutahya outlet-Reservoir 1	14.20	18.80
10	Reservoir 1- Reservoir 2	23.20	32.20
11	Reservoir 2- Reservoir 3	22.32	32.6
12	Reservoir 3- Eskisehir Intake	19.9	24.5
13	Eskisehir Intake-Esenkara	10.9	16.8
14	Esenkara-Eskisehir Outlet	10.2	14.5
15	Eskisehir Outlet-Cavkum	10.8	14.5
16	Cavkum-Alpu Intake	11.03	14.2
17	Alpu Intake-Alpu Outlet	11.04	14.2
21	Yalinli-Yunusemre	7.79	9.19
22	Yunusemre-Bicer Intake	5.71	7.18
23	Bicer Intake- Bicer Outlet	7.8	9.55
24	Bicer Outlet-Sazilar	8.84	10.95
25	Sazilar-Sakarya	7.96	15.41

Table 9. Comparison of the simulated dissolved oxygen, phosphorus and nitrate concentrations for summer (July) and winter (January) before and after the application of the aeration (segments 1-25)

Segment No	1	2	3	4	5	6	7	8
DO (mg/L)								
(July)- Before the aeration	7.89	10.71	11.20	11.21	8.09	7.95	7.47	5.94
(July)- After the aeration	7.89	10.71	11.20	11.21	8.09	7.95	7.47	5.94
(Jan)- Before the aeration	9.42	13.59	14.53	14.56	9.80	9.54	7.82	6.18
(Jan)- After the aeration	9.42	13.59	14.53	14.56	9.80	9.54	7.82	6.18
P (mg/L)								
(July)- Before the aeration	0.03	0.02	0.02	0.02	0.05	0.04	0.03	0.01
(July)- After the aeration	0.03	0.02	0.02	0.02	0.05	0.04	0.03	0.01
(Jan)- Before the aeration	0.02	0.02	0.02	0.02	0.05	0.05	0.10	0.02
(Jan)- After the aeration	0.02	0.02	0.02	0.02	0.05	0.05	0.10	0.02
N (mg/L)								
(July)- Before the aeration	0.99	0.93	0.72	0.71	0.63	0.60	1.00	0.35
(July)- After the aeration	0.99	0.93	0.72	0.71	0.63	0.60	1.00	0.35
(Jan)- Before the aeration	0.78	0.78	0.81	0.82	0.81	0.85	2.98	0.51
(Jan)- After the aeration	0.78	0.78	0.81	0.82	0.81	0.85	2.98	0.51

Segment No	9	10	11	12	13	14	15	16
DO (mg/L)								
(July)- Before the aeration	3.33	14.19	13.32	13.83	7.99	9.05	10.35	10.94
(July)- After the aeration	14.20	23.20	22.32	19.90	10.90	10.20	10.80	11.03
(Jan)- Before the aeration	2.66	18.53	17.86	17.71	10.44	11.92	13.21	13.75
(Jan)- After the aeration	18.80	32.20	32.60	24.50	16.80	14.50	14.50	14.20
P (mg/L)								
(July)- Before the aeration	0.29	0.08	0.06	0.03	0.31	0.31	0.31	0.31
(July)- After the aeration	0.22	0.06	0.05	0.02	0.30	0.27	0.27	0.27
(Jan)- Before the aeration	0.40	0.14	0.14	0.07	0.91	0.92	0.93	0.94
(Jan)- After the aeration	0.30	0.11	0.11	0.05	0.62	0.78	0.79	0.80
N (mg/L)								
(July)- Before the aeration	0.90	0.15	0.34	0.23	0.64	0.63	0.72	0.80
(July)- After the aeration	0.77	0.19	0.33	0.23	0.58	0.57	0.65	0.72
(Jan)- Before the aeration	1.33	0.37	0.83	0.48	1.37	1.62	1.64	1.66
(Jan)- After the aeration	1.13	0.42	0.79	0.47	1.22	1.47	1.49	1.51

Segment No	17	18	19	20	21	22	23	24	25
DO (mg/L)									
(July)- Before the aeration	10.71	4.36	6.62	6.59	7.66	5.62	7.72	8.79	7.93
(July)- After the aeration	11.04	14.20	14.90	11.60	11.70	9.50	8.96	8.92	8.20
(Jan)- Before the aeration	12.99	3.85	7.40	6.98	8.93	6.98	9.41	10.89	15.36
(Jan)- After the aeration	14.20	21.60	23.70	13.30	14.30	12.70	12.20	12.10	16.80
P (mg/L)									
(July)- Before the aeration	0.31	0.51	0.51	0.49	0.49	0.50	0.50	0.50	0.55
(July)- After the aeration	0.27	0.41	0.41	0.39	0.39	0.42	0.43	0.44	0.51
(Jan)- Before the aeration	0.94	1.57	1.59	1.06	1.07	1.09	1.10	1.10	1.52
(Jan)- After the aeration	0.80	1.27	1.28	0.86	0.86	0.88	0.89	0.90	1.34
N (mg/L)									
(July)- Before the aeration	0.81	2.76	2.86	3.23	3.24	3.39	3.35	3.32	2.92
(July)- After the aeration	0.73	2.19	2.27	2.62	2.63	2.76	2.77	2.78	2.61
(Jan)- Before the aeration	1.74	8.28	8.87	6.94	6.99	7.18	7.24	7.29	8.53
(Jan)- After the aeration	1.51	6.63	7.11	5.65	5.68	5.86	5.90	5.94	7.39

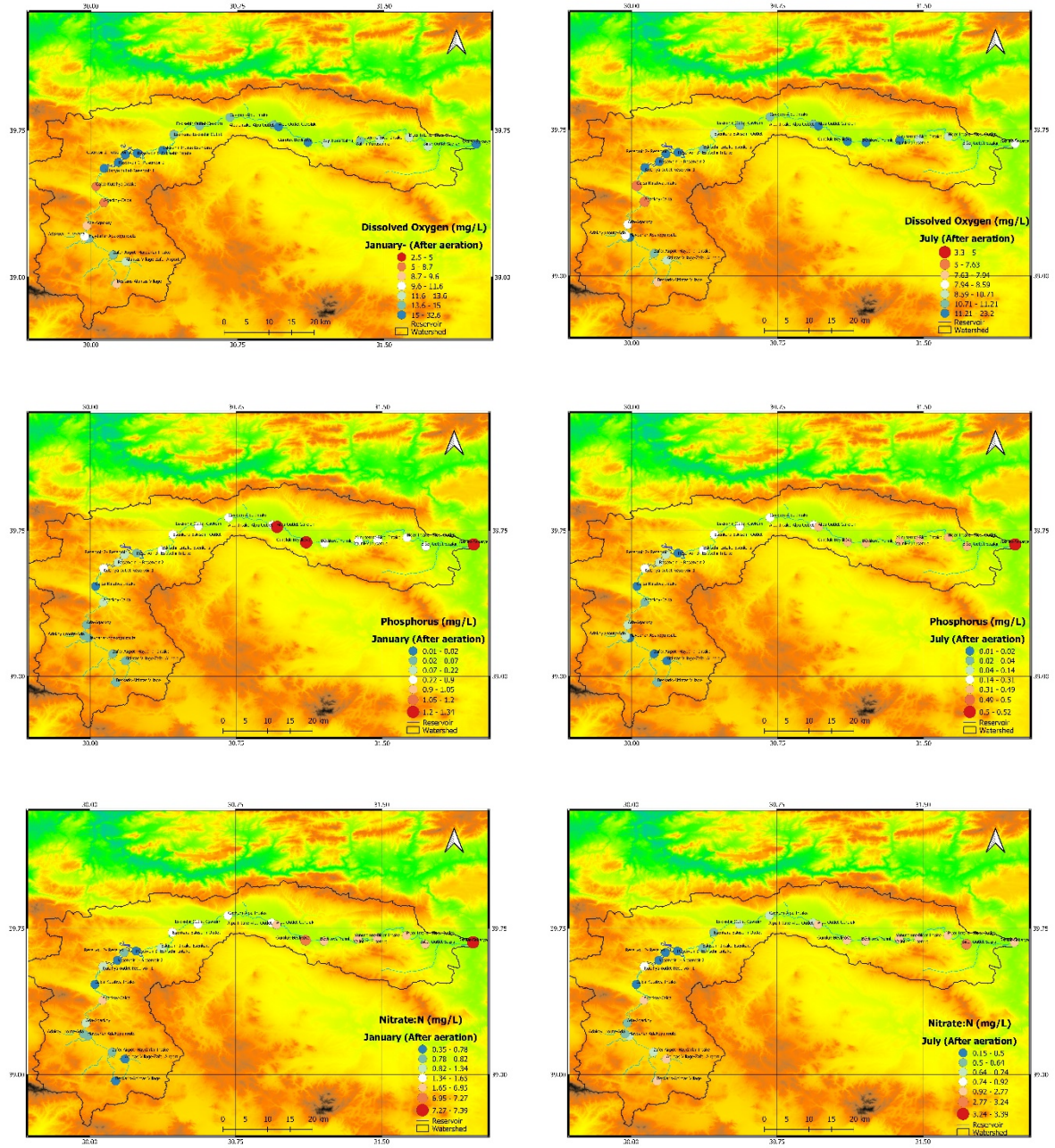

(a) January (b) July

Figure 12. Comparison of the simulated dissolved oxygen, phosphorus, and nitrate concentrations along the river for two different months; a) January, b) July after aeration is applied to the segments.

3.4 Modeling of Chlorophyll-a

Phytoplankton is usually included as a state variable in water quality models such as WASP because of their effects on dissolved oxygen concentrations. When phytoplankton populations exceed established limits, this can be an environmental concern, although the other forms of algae are of equal or greater importance in many water bodies. In this study, the changes in chlorophyll-a concentrations were simulated via the eutrophication module before and after the aeration is applied as mitigation solution in the study site. The calibrated kinematic constants used in modeling of the chlorophyll-a concentrations are given in Table 10.

Table 10. Kinetic constants for modeling of chlorophyll for WASP model calibration (Larico and Medina, 2019)

Parameters	Calibrated Value
Phytoplankton Maximum Growth Rate Constant at 20 C (1/day)	3.5
Phytoplankton Growth Temperature Coefficient	1.068
Phytoplankton Carbon to Chlorophyll Ratio (mg C/mg Chl)	50
Optimal Temperature for Growth (C)	20
Shape parameter for below optimal temperatures	0.004
Shape parameter for above optimal temperatures	0.01
Phytoplankton Respiration Rate Constant at 20 C (1/day)	0.08
Phytoplankton Respiration Temperature Coefficient	1.045
Phytoplankton Death Rate Constant (Non-Zoo Predation) (1/day)	0.1
Nitrogen fixation option (0 no- 1=yes)	1
Phytoplankton Optimal Light Saturation as PAR (watts/m2)	300
Phytoplankton Half-Sat. for Mineralization Rate (mg Phyt C/L)	0.001
Phytoplankton Half-Saturation Constant for N Uptake (mg N/L)	0.4
Phytoplankton Half-Saturation Constant for P Uptake (mg P/L)	0.08
Phytoplankton Half-Saturation Constant for Si Uptake (mg Si/L)	0.1
Phytoplankton Detritus to Carbon Ratio (mg D/mg C)	2.5
Phytoplankton Nitrogen to Carbon Ratio (mg N/mg C)	0.25

Comparison of the simulated chlorophyll-a concentrations before and after the aerations for July and January (Table 11, Figures 13 and 14) indicates a slight decrease in the simulated concentrations after the aeration. The average of simulated chlorophyll-a concentrations for the stream decreased from 1 mg/l to 0.95 mg/l for July and decreased from 1.59 mg/l to 1.42 mg/l for January. Since the aeration was applied after the" Kutahya outlet-Reservoir1" segment (#9), higher values of chlorophyll-a concentrations observed at the upstream stations (1,2,5,6) were not affected.

Table 11. Comparison of the simulated chlorophyll-a concentrations before and after the aerations for July and January

Segment No	Segment Name	Chlorophyll-a-July (mg/L) Before the aeration	Chlorophyll-a-July (mg/L) After the aeration	Chlorophyll-a-January (mg/L) Before the aeration	Chlorophyll-a-January (mg/L) After the aeration
1	Beskaris-Altintas Village	3.05	3.05	2.66	2.66
2	Altintas Village-Zafer Airport	2.17	2.17	2.16	2.16
3	Zafer Airport -Haydarlar Intake	0.92	0.92	1.15	1.15
4	Haydarlar-Adakoyu route	0.76	0.76	1.06	1.06
5	Adakoyu route-Ada	3.35	3.35	3.38	3.38
6	Ada-Agackoy	2.86	2.86	3.67	3.67
7	Agackoy-Calca	0.92	0.92	2.88	2.88
8	Calca-Kutahya Intake	0.54	0.54	0.79	0.79
9	Kutahya outlet-Reservoir 1	0.71	0.53	1.02	0.47
10	Reservoir 1- Reservoir 2	0.27	0.12	0.68	0.22
11	Reservoir 2- Reservoir 3	0.23	0.12	0.49	0.12
12	Reservoir 3- Eskisehir Intake	0.42	0.34	0.56	0.4
13	Eskisehir Intake-Esenkara	0.48	0.39	0.86	0.74
14	Esenkara-Eskisehir Outlet	0.33	0.27	0.86	0.78
15	Eskisehir Outlet-Cavkum	0.32	0.28	0.82	0.76
16	Cavkum-Alpu Intake	0.3	0.28	0.78	0.76
17	Alpu Intake-Alpu Outlet	0.38	0.37	1.06	1.05
18	Alpu Outlet-Guroluk	0.83	0.67	2.36	1.64
19	Guroluk-Beylikova	0.8	0.66	2.28	1.82
20	Beylikova-Yalinli	0.82	0.72	1.6	1.28
21	Yalinli-Yunusemre	0.95	0.88	1.72	1.38
22	Yunusemre-Bicer Intake	1.07	1.01	1.82	1.47
23	Bicer Intake- Bicer Outlet	1.02	0.98	1.76	1.57
24	Bicer Outlet-Sazilar	0.96	0.92	1.69	1.66
25	Sazilar-Sakarya	0.53	0.52	1.57	1.53

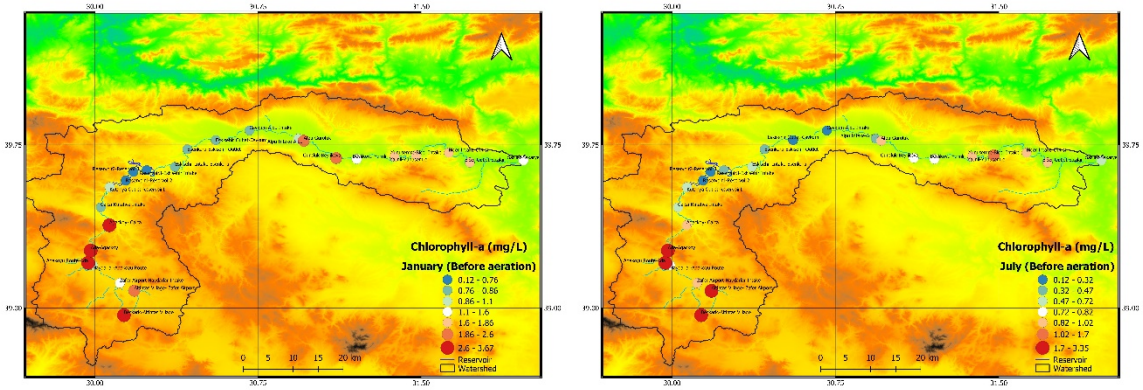

(a) January (b) July

Figure 13. Comparison of the simulated chlorophyll-a concentrations along the river for two different months; a) January, b) July before aeration.

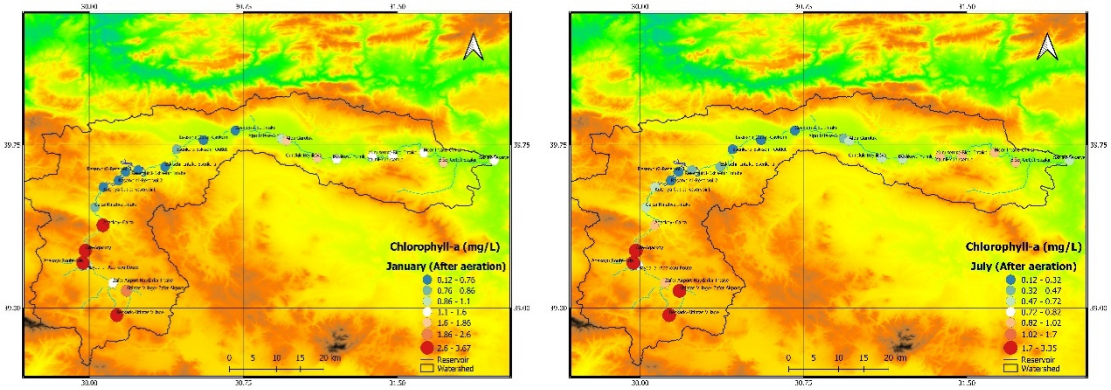

(a) January (b) July

Figure 14. Comparison of the simulated chlorophyll-a concentrations along the river for two different months; a) January, b) July after aeration is applied to the segments.

4. Conclusions

In this study, hydrodynamics and water quality parameters are simulated in the Porsuk River via the application of WASP for the water year 2015. The Porsuk main river is divided into 25 segments, considering available water quality and flow monitoring stations. For calibration of the model, the flow rates monitored at Beskaris, Porsuk Ciftligi, Calca, Esenkara, Parsibey and Kiranharmani stations are used. Following the simulation of discharges at the flow gauging stations accurately, water quality parameters are modeled via the eutrophication module available within the WASP model.

Based on the observed data and the numerical simulations, it can be concluded that the water quality in the Porsuk river is better in the upstream reaches but starts to deteriorate after passing through the province of Kütahya. Dissolved oxygen observations and the numerical model simulations indicate a sudden decrease from 7.56 mg/l to 2.6 mg/l along segment #9.

Water quality then gets better at the reservoir but then another sudden decrease is observed at further downstream at the Alpu-Guroluk segment. Comparison of the simulation results for dissolved oxygen indicated that in both January and July having very different flow regimes, the lowest dissolved oxygen values are observed at specific locations: Kutahya-Reservoir1 segment concentrations of dissolved oxygen are observed as 2.66 in January and 3.33 mg/L in July respectively, and at Alpu-Guroluk (#18) segment as 4.36 mg/L in both months. At these stations, dissolved oxygen stays below the standard limit of 5 mg/L throughout the year.

As a mitigation option, aeration applications at these two stations are proposed and the effects of aeration on the simulated parameters of dissolved oxygen, phosphorus and nitrate concentrations are investigated. Aeration at two segments has significantly improved the dissolved oxygen concentrations whereas it has a more subtle effect on nitrate and phosphorus concentrations.

We also modeled chlorophyll-a concentrations along the stream based on the calibrated flow and water quality model. However, since no observations of chlorophyll-a concentrations is available, simulated data could not be validated. Still, the simulated chlorophyll-a concentrations before and after aeration can be used for evaluating the effects of the aeration. Comparison of the simulated chlorophyll-a concentrations before and after the aeration for July and January indicated a slight decrease in the simulated concentrations after the aeration. The average of simulated chlorophyll-a concentrations for the stream decreased from 1 mg/l to 0.95 mg/l for July and decreased from 1.59 mg/l to 1.42 mg/l for January. These results can be evaluated as an improvement in water quality.

Author Statement

The authors confirm contribution to the paper as follows: study conception and design: Emre Dumlu; data collection: Emre Dumlu; analysis and interpretation of results: Emre Dumlu, Şebnem Elçi; draft manuscript preparation: Emre Dumlu, Şebnem Elçi. All authors reviewed the results and approved the final version of the manuscript.

Conflict of Interest

The authors declare no conflict of interest.

References

Ambrose, R.B., Wool, T., & Martin, J.L. (1993). WASP User's Manual, US Environmental Protection Agency, *Environmental Research Laboratory*, Athens, Georgia.

Alam, A., Badruzzaman, A. B. M., & Ali, M. A. (2013). Assessing Effect of Climate Change on The Water Quality of The Sitalakhya River Using WASP Model. *J. Civ. Eng*, 41, 21-30.

Beutel, M.W., & Horne, A.J. (1999). A Review of The Effects of Hypolimnetic Oxygenation on Lake and Reservoir Water Quality. *Lake and Reservoir Management*, 15(4), 285-297.

Burian, S.J., McPherson, T.N., Brown, M.J., Streit, G.E., & Turin, H.J. (2002). Modeling the Effects of Air Quality Policy Changes on Water Quality in Urban Areas. *Environmental Modeling & Assessment*, 7, 179–190. https://doi.org/10.1023/A:1016328822334

Burigato Costa, C.M.d., da Silva Marques, L., Almeida, A.K., Leite, I.Z., & de Almeida, I.K. (2019). Applicability of Water Quality Models Around The World—A Review. *Environ Sci Pollut Res*., 26, 36141–36162 https://doi.org/10.1007/s11356-019-06637-2.

Burns, F.L., & Powling, I.J. (1981). Destratification of Lakes and Reservoirs to Improve. Water Quality. *Proceedings of a Joint United States/Australia seminar and workshop*., Melbourne, Australia, February 19–24.

Carroll, R.W.H., Warwick, J.J., Heim, K.J., Bonzongo, J.C., Miller, J.R., & Lyons, W.B. (2000). Simulation of Mercury Transport and Fate in the Carson River, *Nevada. Ecol. Model*, 125, 255–278.

Chen, C., Lung, W., Li, S., & Lin, C. (2012). Technical Challenges with BOD/DO Modeling of Rivers in Taiwan. *J. Hydro-Environ Res*., 6.

Chipofya, V.H., &Matapa, E.J. (2003). Destratification of an Impounding Reservoir Using Compressed Air-case of Mudi Reservoir, Blantyre, Malawi. *Physics and Chemistry of The Earth*, 28(20-27), 1161-1164.

Chueh, Y.Y., Fan, C., & Huang, Y.Z. (2021). Copper Concentration Simulation in a River by SWAT-WASP Integration and Its Application to Assessing The Impacts of Climate Change and Various Remediation Strategies. *Journal of Environmental Management*, 279, 111613. https://doi.org/10.1016/j.jenvman.2020.111613.

Croome, R.L. (1981). Artificial Destratification of Two South Australian Reservoirs. *Proceedings of the International Symposium on Artificial Destratification*, Melbourne, 1979, AGPS.

Downing, J.A., Watson, S.B., & McCauley, E. (2001). Predicting Cyanobacteria Dominance in Lakes. *Canadian Journal of Fisheries and Aquatic Sciences*, 58, 1905–1908.

Dumlu, E., & Elçi, Ş. (2022). Application of the Wasp Model for Assessment of Water Quality of the Porsuk River, Turkey. In Ş. Elçi & G. Bombar (Eds.). *14th International Conference on Hydroscience and Engineering,* 177–185. https://www.iche2022.org/_files/ugd/21d103_be56d464954b4310a2461ccf02fd83b9.pdf.

Elçi Ş., Erdem A., & Gokcen G. (2010). Numerical Modeling of the Effects of Kizildere Geothermal Power Plant on Water Quality of the Great Menderes River, Turkey. *Balwois*. https://balwois.com/wp-content/uploads/old_proc/ffp-1977.pdf

Gallagher, J.W., & Jr. (1984). Richard B. Russell Dam and Lake Oxygen Injection System, *Proceedings of a Seminar on Applications in Water Quality Control*, US Army Corps of Engineers, Committee on Water Quality, Washington, DC, 184-190.

Havens, K.E. (2008). Cyanobacteria Blooms: Effects on Aquatic Ecosystems. In: *Hudnell HK ed. Cyanobacterial Harmful Algal Blooms: State of The Science and Research Needs,* New York, Springer, 733–747.

Hickey, C.W., & Gibbs, M.M. (2009). Lake Sediment Phosphorus Release Management—Decision Support and Risk Assessment Framework. *New Zealand Journal of Marine and Freshwater Research*, 43(3). 819-856. doi: 10.1080/00288330909510043.

Holland, J. P., & Tate Jr, C. H. (1984). Investigation and Discussion of Techniques for Hypolimnion Aeration/Oxygenation. *Army Engıneer Waterways Experiment Station Vicksburg*, Ms Hydraulics Lab.

Horne A.J. (2019). Hypolimnetic Oxygenation 1: Win–Win Solution for Massive Salmonid Mortalities in a Reservoir Tailwater Hatchery on the Mokelumne River, California. *Lake Reservoir Manage*, 35(3),308–322.

Horne A.J, & Beutel M. (2019). Hypolimnetic Oxygenation 3: An Engineered Switch from Eutrophic to a Meso/Oligo-trophic State in a California Reservoir. *Lake Reservoir Manage*, 35(3),338–353.

Hyenstrand, P., Blomqvist, P., & Petersson, A. (1998). Factors Determining Cyanobacterial Success in Aquatic Systems—A Literature Review. *Archiv für Hydrobiologie (Special Issues)*, 51, 41–62.

Iqbal, M.M., Shoaib, M., & Agwanda, P., & Lee, J.L. (2018). Modeling Approach for Water-Quality Management to Control Pollution Concentration: A Case Study of Ravi River, Punjab, Pakistan. *Water 10*, 8, 1068. https://doi.org/10.3390/w10081068.

Jia, H., Zhang, Y., & Guo, Y. (2010). The Development of a Multi-Species Algal Ecodynamic Model for Urban Surface Water Systems and its Application. *Ecol. Model*, 221, 1831–1838.

Köse, E., Çiçek, A., Emiroğlu, Ö., Tokatlı, C., Uğurluoğlu, A., Başkurt, S., Aksu, S., & Uylaş, M. (2016). Water Quality Assessment of Porsuk Stream Basin. *Biological Diversity and Conservation*, 9, 119-126.

Kannel, P.R., & Gan, T.Y. (2013). Application of WASP for Modelling and Management of Naphthenic Acids along Athabasca River, Alberta, Canada, *Water Air Soil Pollut*, 224, 1764. https://doi.org/10.1007/s11270-013-1764-1.

Lindenschmidt, K.E., Pech, I., & Baborowski, M. (2009). Environmental Risk of Dissolved Oxygen Depletion of Diverted Flood Waters in River Polder Systems-A Quasi-2D Flood Modelling Approach. *Sci. Environ*. 407, 1598–1612.

Meyer, E.B., Price, R.E., & Wilhelms, S.C. (1992). Destratification System Design for East Sidney Lake, New York. Final report for USACE, Miscallenous Paper, W-92-2. 1979. *Australian Government Publishing Service*,Canberra, 915.

Park, J.Y., Park, G.A., & Kim, S.J. (2013). Assessment of Future Climate Change Impact on Water Quality of Chungju Lake, South Korea, Using WASP coupled with SWAT. J. Am. *Water Resour. Assoc.*,49, 1225–1238.

Obin, N., Tao, H., Ge, F., & Liu, X. (2021). Research on Water Quality Simulation and Water Environmental Capacity in Lushui River Based on WASP Model. *Water*, 13, 2819. https://doi.org/10.3390/w13202819.

Seo, D.I., Kim, M.A., & Ahn, J.H. (2012). Prediction of Chlorophyll-a Changes Due to Weir Constructions in The Nakdong River Using EFDCWASP Modelling. *Environ. Eng.* Res, 17, 95−102.

Shabani, A., Woznicki, S. A., Mehaffey, M., Butcher, J., Wool, T. A., & Whung, P.Y. (2021). A Coupled Hydrodynamic (HEC-RAS 2D) and Water Quality Model (WASP) for Simulating Flood-induced Soil, Sediment, and Contaminant Transport, *Journal of Flood Risk Management*, 14(4), e12747. https://doi.org/10.1111/jfr3.12747.

Soyupak, S., Mukhallalati, L., Yemisen, D., Bayar, A., & Yurteri, C. (1996). Evaluation of Eutrophication Control Strategies for the Keban Dam Reservoir. *Ecol. Model*, 97, 99–110.

Tekkanat, I.S., & Sarış, F. (2015). Long-Term Trends Observed in Stream Flows in the Porsuk Stream Basin (in Turkish). *Turkish Journal of Geography*, 64, 69-83.

Wang, Q., Dai, W., Zhao, X., Li, S., & Zhao, Y. (2009). Numerical Model of Thermal Discharge from Laibin Power Plant Based on Mike 21FM. *China Environmental Science*, 22, 332–336.

Wang, P.F., Martin, J., & Morrison, G. (1999). Water quality and eutrophication in Tampa Bay, Florida. Estuar, *Coast. Shelf Sci*. 49, 1–20.

Wool, T., Ambrose, R.B., Jr., Martin, J.L., & Comer, A. (2020). WASP 8: The Next Generation in the 50-year Evolution of USEPA's Water Quality Model. *Water*, 12, 1398. https://doi.org/10.3390/w12051398.

Scientific Research Communications

Research Article

Sci. Res. Comm. (2022)
Volume 2, Issue 2
doi: 10.52460/src.2022.009

Biological Activities of Plant Ethanolic Extracts from *Asplenium trichomanes* (Maidenhair spleenwort) and *Lagenaria siceraria* (Bottle gourd)

Mohamed Chanfiou Mkouboi[1,*], Syed Nasar Rahaman[2], M.A. Imran Musthafa[2], M. Abdul Jaleel[2]

[1] Ege University, Department of Bioengineering Bornova, 35100, Izmir, Türkiye
[2] The New College (Autonomous), Department of Biotechnology, Royapettah, Chennai 600014, India
[*] Corresponding author: mkouboifils@hotmail.com

Received: 28.07.2022 Accepted: 22.10.2022

Abstract

Plant is commonly known as one of the main dietary sources of the human being. Many plant-derived compounds have been used as drugs, either in their original or semi-synthetic form. There are also several plant extracts or "phytomedicine" in clinical trials for the treatment of various diseases. Plant-derived compounds will still be an essential aspect of the therapeutic array of medicines available to the physician, particularly with the availability of new hyphenated primary analytical methods by determining biological activities of medicinal plants. The ethanolic extracts of two creeper plants namely *Asplenium trichomanes* (Maidenhair spleenwort), *Lagenaria siceraria* (Bottle gourd), originated from different geographical part of the world were chosen to be determine its antimicrobial, antioxidants, anti-inflammatory and UV radiation absorbance activity which is mainly characterize the anticancer activity which is nowadays become the most fatal disease. Such kind of biomedical and biotechnology approaches have been aimed to eradicate naturally such illness which is the main objective of this work. The present study shows that different ethanolic leaf extracts have an important and necessary antioxidant and anti-inflammatory properties with UV absorbing activity at UV –A region. These results show that *Asplenium trichomanes* and *Lagenaria siceraria* will be potential natural sources of antioxidant and anti-inflammatory activity. They could have greater importance as therapeutic agents in preventing or treating oxidative stress and inflammation related disorders, such as cancer and other health disorders. While the negative result of the antimicrobial activity of most of both ethanolic extract is considered as a positive result depending to main purpose of future work. Because it shows that extracts will never upset the gastric flora, in which they must be applied safely away from any harmful reaction and allergic or side effects for the living organism.

Keywords: Medicinal plants, ethanolic extracts, antioxidants, anti-inflammatory, antimicrobial, anticancer, Ultra-violet absorbance activities, Asplenium trichomanes (Maidenhair spleenwort), Lagenaria siceraria (Bottle gourd)

1. Introduction

Cancer is a disease with a multifactorial etiology, resulting mainly from genetic alterations, environmental factors and lifestyle (Popim et al., 2008). Up to 10% of invasive cancers are related to radiation exposure, including both ionizing radiation and non-ionizing radiation

(Anand et al., 2008; Balkwill and Coussens, 2004). Exposure to solar ultraviolet (UV) radiation is a causative factor in skin photocarcinogenesis and photoaging. Cancers due to UV irradiation may be a risk and high in future because of the increase in depletion of the ozone layer.

Sun radiation constantly impacts the earth with approximately 50% visible light (400- 800 nm), 40% infrared radiation (IR) (1300- 1700 nm), and 10% ultraviolet radiation (UV) (10-400 nm). UV is divided conventionally to UV-A (320-400 nm), UV-B (290-320 nm), UVC (100-290 nm), and vacuo UV (10-100 nm) (Mensah et al., 2001). Sunscreens are chemicals that provide protection against the adverse effects of solar and in particular UV radiation (Elmets and Young, 1996). Extracts of many plants have been found to possess chemical compounds which act as anti-inflammatory agents and previous research has shown that inflammation is causally linked to carcinogenesis and acts as a driving force in premalignant and malignant transformation of cells (Gomes et al., 2008).

The search for potent natural antioxidants, especially from plant sources, as phytomedicine has become an important research issue at a world-wide level. Many physicians and researchers now contemplate the use of antioxidant treatments as a key strategy for inhibiting or reversing the process of carcinogenesis (Niki, 2010). Traditional medicines play an important role in health services around the globe. About three-quarters of the world population relies on plants and plant extracts for healthcare. The rational design of novel drugs from traditional medicine offers new prospects in modern healthcare. (Singh and Singh, 2008; Prachayasittikul et al., 2008; Shah et al., 2010; Brown et al., 2018; MacDonalds-Wicks et al., 2006; Regoli and Winston, 1999; Stevenson and Hurst, 2007; Halim et al., 2022).

1.1 *Asplenium Trichomanes* (Maidenhair Spleenwort)

Asplenium trichomanes subsp. *trichomanes* is a fern with clusters of 5 to 25 cm long fronds arising from a short, thick rhizome. The small pinnae curl under in dry times though the fern quickly recovers when moisture becomes available. When fertile, ripe sporangia can cover the lower surface of the pinnae (Duncan and Isaac, 1986). The fern can re-sprout from its thick rhizome following fire or other damage. It can be identified year-round, arises from a short, thick rhizome covered with very dark, shiny, coarse, lattice-like scales. Fronds are clustered, erect and 5 to 25 cm long. The stipe is short, brittle, shiny, black and flattened above, with a tuft of scales at its base. The lamina is deep green, linear, pinnate and firm in texture. The rachis is shiny, blackish, brittle and grooved with narrow, fragmented wings. There are 15 to 40 pairs of shortly stalked pinnae arranged asymmetrically. The pinnae are oblong to oval, 4 to 10 mm long with deeply crenate to almost entire margins. The veins are obscure but minor veins branch pinnately from the midvein. After 6 to 12 months, the lower pinnae are often deciduous leaving small projections. Sori on the undersurface of pinnae are arranged in 3 to 6 pairs along the minor veins, oblique to the midvein. Each sorus is protected by a pale, thin indusium with an irregular margin, opening towards the center of the pinna.

1.2 *Lagenaria Siceraria* (Bottle Gourd)

The genus name *Lagenaria* comes from lagena, the Latin name for a Florence flask; referring to the fruit of *Lagenaria siceraria*. The species name *siceraria* probably also refers to the fruit which is useful when it is mature and dry (siccus). Cucurbitaceae family consists of about 120 genera and 735 species. Plants grow mostly tropical and subtropical countries. Many species are cultivated as food plants such as cucumber, melon, pumpkin and watermelon. The plants are perennial herbs and shrubs. The leaves are alternate flowers are mostly unisexual and white or yellow in color; they occur on the same plant (monoecious) or on separate plants (dioecious). The fruit is berry (soft-shelled) or gourd (hard-shelled) with one to many, the seeds are flattened. The genus *Lagenaria* contains six species, probably all originally Old World and

mainly African. Only two species are found in southern Africa; *Lagenaria siceraria* and *L. sphaerica*. (Deshpande et al., 2008)

The increase in prevalence of multiple drug resistance has shown the development of new synthetic antibacterial, anti-oxidative and anti-inflammatory drugs; moreover, the new drug is necessary to search for new antimicrobial, antioxidant and anti-inflammatory sources from alternative sources. Phytochemicals from medicinal plants showing antimicrobial, antioxidant and anti-inflammatory activities have a potential of filling this need because their structures are different from those of the more studied plants (Miguel, 2010). In this growing interest, many of the phytochemical bioactive compounds from medicinal plants have shown many pharmacological activities (Thakur et al., 2013).

2. Materials and Methods

The leaves of *Lagenaria siceraria*, were collected during the month of December, 2013 from The New College Hostel Campus, Royapettah, Chennai, Tamil Nadu, India. Leaves of *Asplenium trichomanes* were collected from Mbeni, Comoros Islands in Africa. Leaves of these plants were brought to Department of Biotechnology, The New College, Chennai, and were washed with sterile distilled water, then shredded into small fragments. The materials were then shade dried at ambient temperature of 32°C for 21 days. The dried samples were then crushed into fine powder using an electronic blender, screened through 1 mm sieve and packed in sterile pouches.

Six experiments were conducted on these samples in order to determine their characteristics. The materials used and the procedures are given below.

2.1 Solvent Extraction

The fine powder of the leaves of *Asplenium trichomanes*, *Lagenaria siceraria* was extracted at 47°C by using soxhlet apparatus using ethanol as solvent (10g in 150ml of ethanol) for 8 hours. After extraction, the dark solution that was obtained was transferred to 250 ml beaker and dried at room temperature for one week by allowing the ethanol to evaporate. After evaporation the extract that was sticked to the beaker was obtained by scraping with the help of a blade and the amount obtained was weighed in a digital weighing balance and stored properly for further studies.

2.2 Phytochemical Analysis

Phyto-chemical analysis was used to determine various phyto-chemicals present in the leaf extracts of *Asplenium trichomanes*, *Lagenaria siceraria*. Test tubes, test tube holders, micropipettes, respective reagents and chemicals, weighing balance, beakers, conical flasks, distilled water and boiling water bath were used in this experiment. Considering alkaloids, to 1ml of extract, diluted hydrochloric acid and Mayer`s reagent was added to form white precipitate. Considering steroids, for Salkowski reaction, to 2ml of extract 2ml of chloroform and 2ml of concentrated sulfuric acid were added. By shaking well, chloroform layer appears red and acid layer shows greenish yellow florescence. Considering coumarins, to 1ml of the extract, 1ml of 10% sodium hydroxide was added to form yellow color. Considering tannins, to 1ml of the extract, 5ml of distilled water and few drops of 1% lead acetate was added to form white precipitate.

Considering saponins, to 1ml of the extract, 5ml of water was added and shaken vigorously to form honey comb like froth. Considering flavonoids (Shinadow's test), to 1ml of the extract, 5ml to 10 drops of diluted HCl and small amount of zinc or magnesium was added and boiled for few minutes to form reddish pink color. Considering anthraquinones (Borntrager's test), 1ml of the extract was macerated with ether and filtered. To the filtrate, aqueous ammonia was

added to form Pink red or violet color after shaking. Considering phenols, to 1ml of the extract, 2ml of distilled water and few drops of 10% aqueous ferric chloride were added to form blue or green color.

2.3 Determination of UV–Absorbance and %T (Transmittance) at UV-A Range

The leaf extracts of *Asplenium trichomanes*, *Lagenaria siceraria* were prepared at a concentration of 2mg/ml in distilled water. The absorbance and transmittance of both leaf extracts were measured at UV–A range (i.e., from 350nm–380nm) using ELICO SL-150 UV-Vis Spectrophotometer, and their absorbance (OD) and transmittance (%T) values were recorded.

2.4 In-Vitro Antioxidant Study of Leaf Extracts

For the determination by reducing power method, test tubes, ferricyanide reagent, ferric chloride reagent, trichloro acetic acid reagent, phosphate buffer solution, centrifuge tubes, centrifuge machine UV-visible spectrophotometer, quartz cuvettes, distilled water, beakers, conical flasks, and test tube holders were used.

In this experiment, the reducing power of different extracts (20 -100 µg/ml) in 1.0ml of deionized water were mixed with phosphate buffer (2.5ml, 0.2M, Ph 6.6) and 1% potassium ferricyanide (2.5ml). The mixture was incubated at 50^{o}C for 20min. Aliquots of trichloroacetic acid (2.5ml, 10%) were added to the mixture, which was then centrifuged at 1036×g for 10min. The upper layer of solution (2.5ml) was mixed with distilled water (2.5ml) and a freshly prepared $FeCl_3$ solution (0.5ml, 0.1%).

The absorbance was measured at 700nm and the results of anti-oxidant activity of extract of *Asplenium trichomanes* and *Lagenaria siceraria* using reducing power determination method. In this assay, ascorbic acid was used as control and the Optical Density (OD) values were compared with the sample values.

2.5 In-Vitro Anti-Inflammatory Property

For the Inhibition of albumin denaturation, test tubes, beakers, conical flasks, thermometer, bovine serum albumin reagent, water bath, 1N hydrochloric acid, distilled water, and spectrophotometer were used.

Methods of Mizushima and Kobayashi (1968) and Sakat et al. (2010) were followed with minor modifications. The reaction mixture was consisting of test extracts and 1% aqueous solution of bovine albumin fraction, pH of the reaction mixture was adjusted using small amount at 37^{0}C HCl. The sample extracts were incubated at 37^{0}C for 20 min and then heated to 51^{0}C for 20 min. After cooling the samples, the turbidity was measured spectrophotometrically at 660nm. The experiment was performed in triplicate to obtain the percent inhibition of albumin denaturation. In this assay, aspirin was used as control at a concentration of 100µg/ml and the OD value was compared with the leaf extract samples.

Percent inhibition of protein denaturation was calculated as in Eq. (1):

$$\% \text{ inhibition} = [\{\text{Abs control} - \text{Abs sample}\}/\text{Abs control}] \times 100 \quad (1)$$

where, *Abs control* is the absorbance without sample and *Abs sample* is the absorbance of the sample extract/standard.

2.6 Antimicrobial Activity

Table 1 displays the media composition antimicrobial activity experiment. The materials used were, Mueller-Hinton agar plates, antibiotic discs forceps, 18- to 24-hour old pure culture of the organism to be tested, vortex, sterile swabs, inoculating loop, and Bunsen burner.

Table 1. Media composition for Mueller-Hinton agar per liter of distilled water

Beef, infusion from	300.0 g
Casamino acid, technical	17.5 g
Starch	1.5 g
Agar	17.0 g

Antimicrobial discs were purchased from a reputable supplier, HIMEDIA. Sealed cartridges containing commercially prepared paper discs were stored at either 8°C or frozen at -14°C in a non-self-defrosting freezer. Semiautomatic disc dispensers were used to place the disc on Muller Hinton Agar. A 0.5 McFarland standard was prepared.

The steps of the procedure were (1) Preparation of Mueller-Hinton plate, (2) Preparation of inoculum, (3) Inoculum application, (4) Inoculation of the Mueller-Hinton plate, (5) Placement of the antibiotic discs, (6) Displacement, (7) Incubation of the plates (at a temperature range of 35°C ± 2°C), (8) Measuring zone sizes.

3. Results

3.1 Solvent Extraction

Ethanolic extracts of *Asplenium trichomanes* and *Lagenaria siceraria*, were obtained by soxhlet extraction and they were weighed and dissolved to prepare stock solutions of various concentrations according to Table 2.

Table 2. The concentrations of the stock solutions

Asplenium trichomanes	1gm/ml
Lagenaria siceraria	1gm/ml

3.2 Phytochemical Analysis

Phytochemical analysis was carried out for the determination of various chemical compounds and the results were depicted in Table 3.

Table 3. Results of the phytochemical analysis

S. No	Compound	*Asplenium trichomanes*	*Lagenaria siceraria*
1	Alkaloids	Present	Present
2	Steroids	Present	Present
3	Coumarins	Present	Present
4	Saponins	None	Present
5	Phenolics	Present	Present
6	Flavonoids	Present	Present
7	Tannins	None	None
8	Anthroquinones	None	None

3.3 Determination of UV–Absorbance and %T (Transmittance) at UV-A Range

The UV light absorption and transmittance of both extracts was recorded at UV-A range from 350nm to 380nm and the results were recorded and depicted in Table 4.

Table 4. UV–absorbance and %T (Transmittance) at UV-A range

S. No	UV Range (nm)	*Asplenium trichomanes*		*Lagenaria siceraria*	
		OD	%T	OD	%T
1	350	0.780	16.6	1.746	2.0
2	360	0.584	26.1	1.154	7.0
3	370	0.450	36.4	0.714	19.4
4	380	0.364	43.2	0.461	34.6

3.4 In-Vitro Antioxidant Study of Leaf Extracts

The absorbance was measured at 700 nm and the results of anti-oxidant activity of extract of *Asplenium trichomanes* and *Lagenaria siceraria* were determined from the ferric reducing activity. The results are compared in Figure 1.

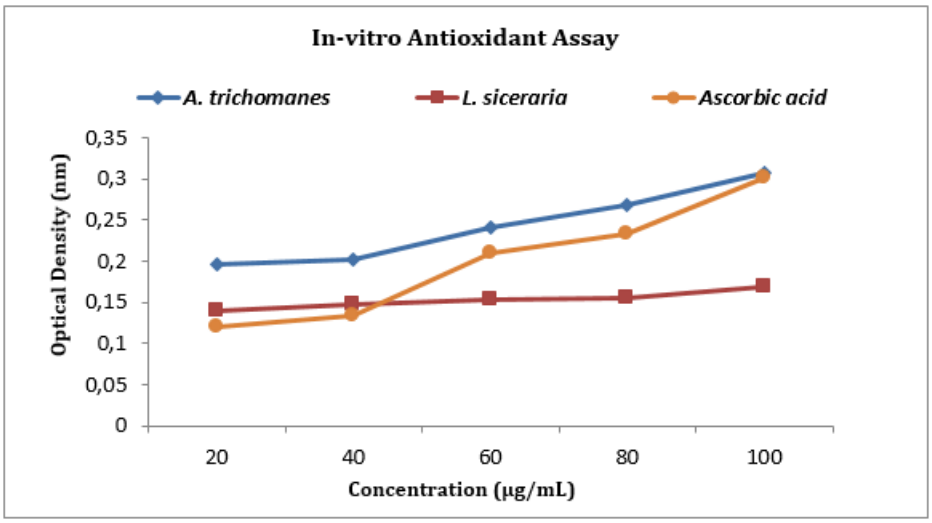

Figure 1. Anti-oxidant activity determination by reducing power method

3.5 In-Vitro Anti-Inflammatory Property

The percent inhibition of albumin denaturation was determined by reading the color (Figure 2) at 660nm and the absorbance values were recorded. The percent inhibition values of the samples were depicted in Table 5.

Table 5. Optical Density for in-vitro anti-inflammatory assay

S. No	Concentration (in µg/ml)	*Asplenium trichomanes*	*Lagenaria siceraria*
1	100	0.324 ± 0.00058	0.297 ± 0.00058
2	200	0.280 ± 0.00058	0.234 ± 0.00058
3	300	0.264 ± 0.00058	0.224 ± 0.00058
4	400	0.244 ± 0.00058	0.203 ± 0.00058
5	500	0.179 ± 0.00058	0.183 ± 0.00058
Control		0.401	
Aspirin (100µg/ml)		0.120	

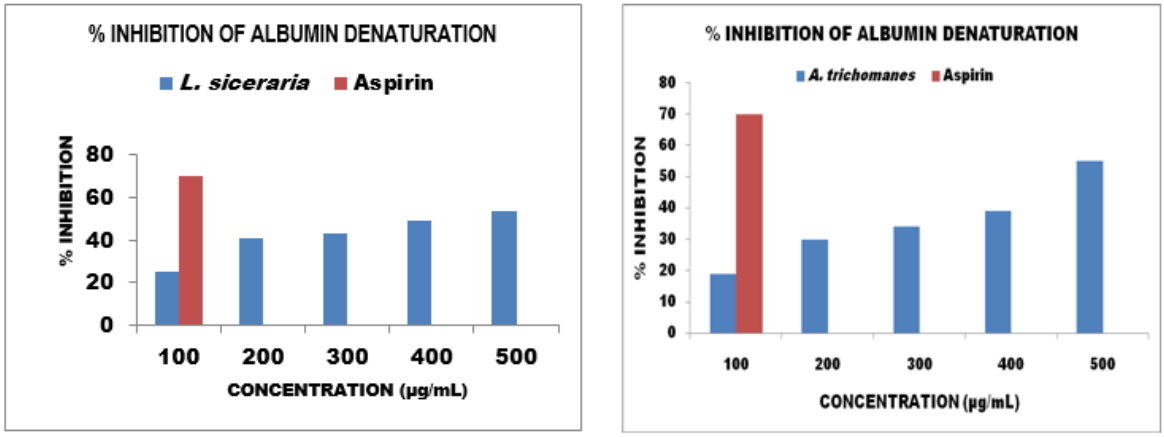

Figure 2. Percent inhibition of albumin denaturation of the extracts

3.6 Antimicrobial Activity

The antimicrobial activity of both plant extracts against *Escherchia coli, Salmonella typhi*, and *Pseudomonas aeruginosa* were recorded from the formation of zones size. It has been found that the antimicrobial activity of the plant extracts shows minimum zone of inhibition.

4. Discussion

Increase in reports about cancer is a serious challenge to the health of the population of the world, and particularly the rate of skin carcinoma is found to be high and the impacts are worsening day by day. The UV radiations are found to be an important factor in causing skin carcinoma and leukemia. Epidemiology and experimental studies have implicated oxidative cellular damage arising from an imbalance between free radical generating and scavenging systems as the primary cause of cancer and various diseases.

The extraction method for the two creepers was applied by the soxhlet apparatus with ethanol as solvent only. This leads to determination of polar compound, further studies are supposed to determine all the compounds by using different type of solvents. The qualitative determination of potent phytochemicals leads to prove the antioxidant activity of plants, it is the case of phenols, flavonoids, tannins, saponins etc…

The antioxidant activity shown by *Asplenium trichomanes* which has been originated from Comoros Islands. A moderate anti-inflammatory activity was specifically determined in the ethanolic *Lagenaria siceraria* which is originated from Chennai-India. This quantitative variation can be explained by the growth media and conditional climate of the plants which provide generally the sufficient nutrients available and sufficient for such kind of characteristics. Most of these plant extracts possess an anti-inflammatory activity which is approximately more than 50%.

Albumin protein denaturation know as coagulation is defined as the process in which proteins lose their tertiary structure and secondary structure by application of external stress such as heat and strong acid or base. The external stress used in this work was the heat which normally leads to the coagulation of protein. This change of characteristic is considered as the inflammation condition.

Owing to that, the addition of the plant extract which react with protein to inhibit coagulation of Albumin which will express a high transparence of the light while using the spectrophotometer. This high transparence defines a low absorbance of the light which will be less than the control absorbance and give a good result while applying the mathematic formula of the inhibition. It was effective in inhibiting heat induced albumin denaturation.

Inhibition of 54%, 55% were respectively observed at 500µg of *Lagenaria siceraria* and *Asplenium trichomanes* extracted in 1ml of ethanol. Aspirin as a standard anti-inflammation drug showed the maximum inhibition 70% at the concentration of 100µg/ml compared with control. The negative result of the antimicrobial activity of both ethanolic extract is considered as a positive result depending to main purpose of future work. Because it shows that both of these extracts will never upset the gastric flora, in which they must be applied safely away from any harmful reaction and allergic or side effects for the living organism.

The combination of these different medicinal plants is expected to produce a high and effective reaction against cancer and other cardio-vascular diseases. Above discussion support that there may be the presence of different polyphenolic compounds such as flavonoids, tannins, terpenoids, phenols, Saponins which are necessary components characterizing the antioxidant and anti-inflammatory properties of drugs.

5. Conclusion

The present study shows that different ethanolic leaf extracts have important and necessary antioxidant and anti-inflammatory properties with UV absorbing activity at UV –A region. These results showed that *Asplenium trichomanes* and *Lagenaria siceraria* could be potential natural sources of antioxidant and anti-inflammatory activity. They could have greater importance as therapeutic agents in preventing or treating oxidative stress and inflammation related disorders, such as cancer and other health disorders. Further studies are planned to be achieved by determining the UV stability of these plants, and to assess the in- vivo biological activities. This will lead to determine the active component characterizing these different biological activities.

Acknowledgments

The authors would like to thank Prof. Dr. Sultan Ahmed İsmail for his support and orientation, to the former Head of Department of Biotechnology The New College Dr. Abdul Sabur, and to all the administration of the New College Royapettah Chennai India. My thanks to all my family especially to my elder brother Abdoulwakil Mkouboi for the financial support of all my graduate studies.

Author Statement

The authors confirm contribution to the paper as follows: study conception and design: S. N. Rahaman, M. A. I. Musthafa; data collection: M. C. Mkouboi; analysis and interpretation of results: All Authors; draft manuscript preparation: M. C. Mkouboi. All authors reviewed the results and approved the final version of the manuscript.

Conflict of Interest

The authors declare no conflict of interest.

References

Anand, P., Kunnumakkara, A.B., Sundaram, C., Harikumar, K.B., Tharakan, S.T., Lai, O.S., Sung, B., &Aggarwal, B.B. (2008). Cancer is a Preventable Disease That Requires Major Lifestyle Changes. *Pharm Res*., 25(9), 2097-2116, doi: 10.1007/s11095-008-9661-9.

Balkwill, F., & Coussens, L. (2004). An Inflammatory Link. *Nature,* 431, 405–406, doi:10.1038/431405a.

Brown, M. J., Sharma, P., Mir, F., Bennett, P. N., & Laurence, D. R. (2018). *Clinical Pharmacology* (Twelfth). Elsevier.

Deshpande, J.R., Choudhari, A.A., Mishra, M.R., Meghre, V.S., Wadodkar, S.G., & Dorle, A.K. (2008). Beneficial Effects of Lagenaria Siceraria (Mol.) Standley Fruit Epicarp in Animal Models. *Indian Journal of Experimental Biology,* 46, 234-242.

Duncan, B.D., & Isaac, G. (1986). Ferns and Allied Plants of Victoria, Tasmania and South Australia, *Melbourne University Press*: *Melbourne*.

Elmets, C.A. & Young, C. (1996). Sunscreens and Photocarcinogenesis: An Objective Assessment. *Photochemistry and Photobiology*, 63, 435-439.

Gomes, A., Fernandes, E., Lima, J.L., Mira, L., & Corvo, M.L. (2008). Molecular Mechanisms of Anti-Inflammatory Activity Mediated by Flavonoids. *Curr Med Chem.*, 15(16), 1586-605, doi: 10.2174/092986708784911579.

Halim, R., Sherzay, N., Faqeryar, N., & Hashimi, M.H. (2022). Quantification of Afghan Saffron's Moisture and Main Compounds (Crocin, Picrocrocin and Safranal) for Quality Evaluation. *Scientific Research Communications*, 2(1), 8, doi:10.52460/src.2022.003

MacDonalds-Wicks, L.K., Wood, L.G., & Garg, M.L. (2006). Methodology for The Determination of Biological Antioxidant Capacity in Vitro: a Review. *Journal of the Science of Food and Agriculture*, 86, 2046-2056.

Mensah, A.Y., Sampson, J., Houghton, P.J., Hylands, P.J., Westbrook, J., & Dunn, M. (2001). Effects of Buddleja Globosa Leaf and Its Constituents Relevant to Wound Healing. *Journal of Ethnopharmacology,* 77,216-221.

Miguel, M.G. (2010). Antioxidant Activity of Medicinal and Aromatic Plants: A Review. *Flavour and Fragrance Journal*, 25(5), 291-312.

Mizushima, Y., & Kobayashi, M. (1968). Interaction of Anti-Inflammatory Drugs with Serum Proteins, Especially with Some Biologically Active Proteins. *Journal of Pharmacy and Pharmacololy*, 20, 169-73.

Niki, E. (2010). Assessment of Antioxidant Capacity in Vitro and in Vivo. *Free Radical Biology & Medicine*, 49(4), 503-515.

Popim, R.C., Corrente, J.E., Marino, J.A.G., & Souza, C.A. (2008). Skin Cancer: Use of Preventive Measures and Demographic Profile of a Risk Group in The City of Botucatu. *Science Collective Health*, 13(4), 1331-1336, doi.org:10.1590/S1413-81232008000400030.

Prachayasittikul, S., Buraparuangsang, P., Worachartcheewan, A., Isarankura-Na-Ayudhya, C., & Ruchirawat, S. (2008). Antimicrobial and Antioxidative Activities of Bioactive Constituents from Hydnophytum Formicarum Jack. *Molecules*, 13(4), 904-921, doi: 10.3390/molecules13040904.

Regoli, F., & Winston, G.W. (1999). Quantification of Total Oxidant Scavenging Capacity of Antioxidants for Peroxynitrite, Peroxyl Radicals, and Hydroxyl Radicals. *Toxicology and Applied Pharmacology*, 156(2), 96-105.

Sakat, S.S., Juvekar, A.R., & Gambhire, M.N. (2010). In Vitro Antioxidant and Anti-Inflammatory Activity of Methanol Extract of Oxalic Corniculata Linn. *International Journal of Pharmacy and Pharmaceutical Sciences*, 2, 146-156.

Shah, B.N., Seth, A.K., & Desai, R.V. (2010). Phytopharmacological Profile of *Lagenaria Siceraria*: A Review. *Asian Journal of Plant Sciences*, 9, 152-157, doi: 10.3923/ajps.2010.152.157

Singh, S., & Singh, R.P. (2008). In Vitro Methods of Assay of Antioxidants: An Overview. *Food* Reviews *International*, 24:4, 392-415, doi: 10.1080/87559120802304269

Stevenson, D.E., & Hurst, R.D. (2007). Polyphenolic Phytochemicals-Just Antioxidants or Much More? *Cellular and Molecular Life Sciences*, 64, 2900-2916, doi: 10.1007/s00018-007-7237-1

Thakur, R., Yadav, K., & Khadka, K.B. (2013). Study of Antioxidant, Antibacterial and Anti-Inflammatory Activity of Cinnamon (Cinamomum Tamala), Ginger (Zingiber Officinale) and Turmeric (Curcuma Longa). *American Journal of Life Sciences*, 1(6), 273-277, doi: 10.11648/j.ajls.20130106.16

Scientific Research Communications

Research Article

Sci. Res. Comm. (2022)
Volume 2, Issue 2
doi: 10.52460/src.2022.010

Effects of Bio-Particles on Mechanical and Quasi-Static Punch Shear Behaviors of Glass/Epoxy Composites

Halis Kandaş* **Okan Özdemir**

Dokuz Eylül University, Department of Mechanical Engineering, Tınaztepe Campus, Izmir, Türkiye
* Corresponding author: haliskandas1@gmail.com

Received: 09.08.2022 Accepted: 06.12.2022

Abstract

In this study, the effect of acorn powder reinforcement at different percentages on the mechanical and quasi-static penetration behavior of glass fiber reinforced composites was investigated. Reinforcement materials used are woven E-glass fiber and cleaned acorn micro powders. Powders were cleansed from impurities with a sodium hydroxide solution. Cleaned powders were mixed with resin by using a mechanical mixing method. Thereafter, resin mixture was applied to glass fibers with hand lay-up method and composite plate was produced by vacuum bag method. Quasi-static penetration tests were performed at room temperature as well as mechanical tests. While 1, 10 and 20 mm/min were selected as quasi-static penetration test speed, tension, compression and three point bending tests were selected as mechanical tests. Force and energy test results of quasi-static penetration tests of composites were compared with each other. Additionally, tensile, compressive and flexural strengths of the composites were investigated.

Keywords: Particle reinforced composites, bio-composites, glass fiber

1. Introduction

Commonly, composite materials are mostly made of petrochemical-based materials. However, these materials pose a serious environmental pollution problem due to their long dissolve time in nature (Bledzki and Jaszkiewicz, 2010). Therefore, bio-composites produced using biodegradable and renewable natural materials have been recently preferred (Kılınç et al., 2016). While forests are considered as the most important sources of natural materials, they are disappearing due to extreme usage of wood. For this reason, current investigations on the use of natural materials have focused on side product materials of forests and wood industry as a reinforcement material (Agayev and Özdemir, 2019). In various studies, natural products such as almond shell (Essabir et al., 2013), walnut shell (Zahedi et al., 2013), coconut shell (Bledzki et al., 2010) and vine stem (Kılınç et al., 2016) have been also used as fillers in manufacturing composite materials.

When the studies in the literature are examined, it is observed that different fiber and particle reinforcements are used rarely together as a reinforcement material. In these studies, it was concluded that different proportions of particle reinforcements positively affect the mechanical properties of fiber-reinforced composites (Singh and Rawat, 2018).

Recently, many researches have performed a study on composites with different material stacking sequences under various loading rates and boundary conditions. These researches concluded that laminated composite structures are sensitive to impact loadings of external loading conditions (Taghizahed et al., 2018). As a result, impact properties of glass/epoxy composites have been an important subject of many researches for recent years. The main goal in these researches is optimizing these materials for usage of different applications by understanding their characteristic properties and energy dissipating impact damage mechanisms (Erkendirici and Haque, 2012). Even though, many researches considered the impact loading as one of the most critical loading type. Due to its different damage responses, investigating low and high velocity impact are seen as a complicated task. Because of that using quasi-static punch shear test which has the same failure mechanisms, considered as a better option (Sadeghi and Pol, 2019). The researchers explained the ballistic behavior of composites as five stages in their study. These phases are listed as impact–contact and stress wave propagation, hydrostatic compression and local punch shear, shear plug formation under compression-shear, large deformation under tension-shear, and end of penetration. In addition, they stated that these stages could be examined better by using the force-deformation data obtained from the quasi-static punch shear test (Gama and Gillespie, 2008).

In this study, composite materials with both fiber and particle reinforcement were used. Acorn powder, which is a natural reinforcement material, was used as a particle reinforcement material at different ratios. Plain-woven laminates were also used as fiber reinforcement material. Because of the above reasons, quasi-static punch shear test responses of composites were investigated at different particle ratios, along with mechanical properties of composites.

2. Methodology

Particle and fiber reinforced composites were manufactured in this study. In the manufacturing of composites, 10-40 μm acorn powder was used as particle material and woven glass laminates with 500gr/m² were used as fiber material. F-1564 epoxy and F3487 hardener were used as the matrix material. The materials used in the manufacturing of composite panels are shown in Figure 1.

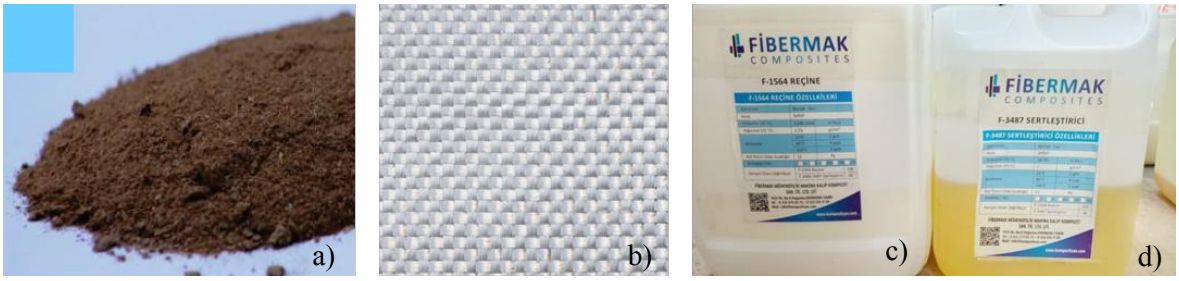

Figure 1. a) Acorn powder, b) woven glass fiber, c) F-1564 epoxy, d) F3487 hardener

Acorn powder was cleansed from impurities since it is a natural material. Grinded acorn powder was chemically treated in a 1.6mol 1-1 i sodium hydroxide aqueous solution for 48 hour. Hence, acorn powder was cleansed from contamination such as dust, corrosive organisms, natural residues and other materials. Purified acorn powder was left to dry for 96 hours before manufacturing of composite materials (Agayev and Ozdemir, 2019). Apart from this cleaning method, Ethylenediaminetetraacetic acid (EDTA) and polyethyleneimine (PEI) (Sigma–Aldrich, Seeze, Germany) can also be used for this process (Le Troedec et al., 2008). Acorn powder cleaning process are given in Figure 2.

Figure 2. Acorn powder cleaning process

Prepared acorn powder wase added to the respective epoxy resin and hardener and mixed mechanically at room temperature. The mixing ratio of hardener - epoxy resin is 1:3. In manufacturing of composites, hand lay-up method was preferred. The fiber content in the composite is 44% by weight. Firstly, the matrix-particle mixture were applied equally to each layer of composites in order to ensure homogeneous disturbance of particle. The vacuum tubes were connected to both ends of the structure in order to ensure balanced vacuum distribution in the later stages of the production process. After that, these composite laminates were vacuum bagged by a device from Dokuz Eylül University, as shown in Figure 3. Vacuum-bagged structure was left to curing for 8 hours at 80°C according to the instructions of matrix material.

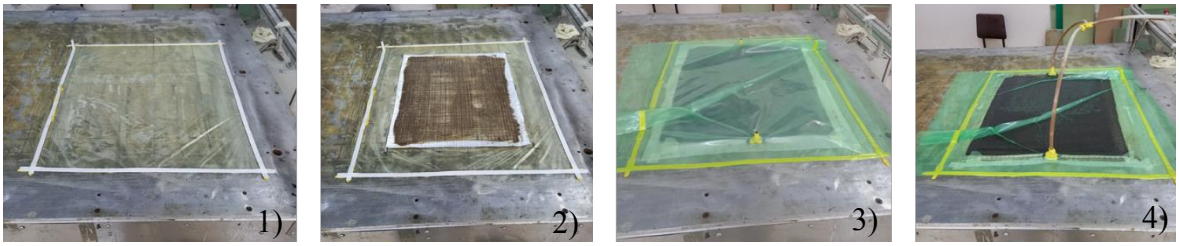

Figure 3. Composite plate manufacturing processes

After particle and fiber reinforced composite plates were manufactured, they were cut to the specimen sizes. Sizing process was performed by using a water refrigerated diamond blade Manufactured composite test specimens are given in Figure 4.

Figure 4. Manufactured composite test specimens

Tension, compression and three point bending tests were carried out at 1mm/min speed. The dimension of test specimens are 205x25 mm, 140x13 mm and 85x13 mm, respectively. In addition to mechanical tests, quasi-static punch-shear tests were also executed. Quasi-static punch-shear tests were carried out on 100x100 mm samples using a test apparatus with a clamp diameter of 76 mm. The cross head used in the quasi-static punch-shear tests is hemi-spherical shaped equipment with 12.7 mm head diameter. Quasi-static punch-shear tests were executed at 1, 10 and 20 mm/min cross head speed at room temperature. Tests were carried out at Shimadzu universal testing machine in Dokuz Eylül Mechanical Engineering Department. Each mechanical test was performed at least 5 times. The equipment that were used in the experiments are given in Figure 5.

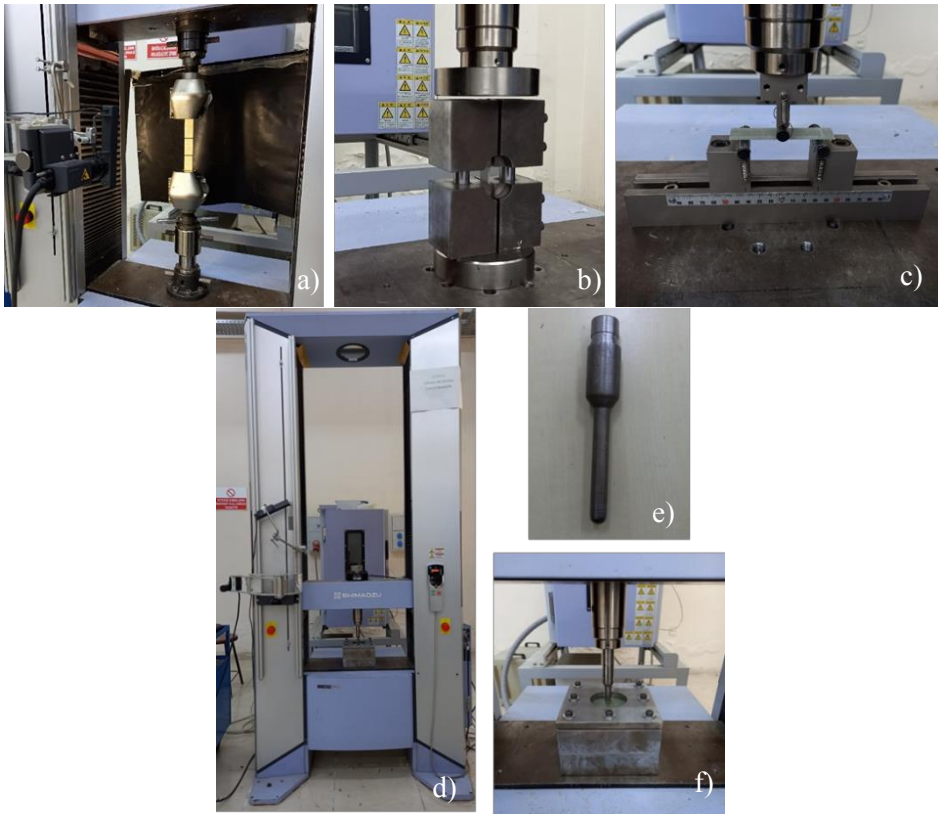

Figure 5. Experimental test setups of a) tensile, b) compression, c) three-point bending, d, e, f) quasi-static indentation tests

3. Results and Discussions

This research focuses on effect of acorn particle reinforcements in glass fiber reinforced composites. Tensile, three point bending and compression tests were performed in order to investigate the mechanical behavior of composites. Through mechanical tests, tensile strength, flexural strength and compressive strength of composites were determined along with tensile modulus and flexural modulus of composites. The mechanical properties of the composites are given in Figure 6. It can be observed from the figure that, tensile and compressive strength of composites increases until 2% particle ratio and then drops at 3% particle ratio. However, flexural strength, unlike tensile and compressive strength, shows a continuous increment trend with increasing the particle ratio. According to the Figure 6, while tensile modulus of composites starts to decrease after 1% particle ratio, flexural modulus of composites decreases after 2% particle reinforcement ratio.

Table 1. Mechanical strengths and modulus of acorn reinforcement specimens

	Tensile Strength (MPa)	Tensile Modulus (GPa)	Flexural Strength (MPa)	Flexural Modulus (GPa)	Compressive Strength (MPa)
0%	334	18.6	402	16.4	209
1%	351	20.8	416	17.5	232
2%	373	19.5	423	17.6	247
3%	286	19.4	456	17.3	226

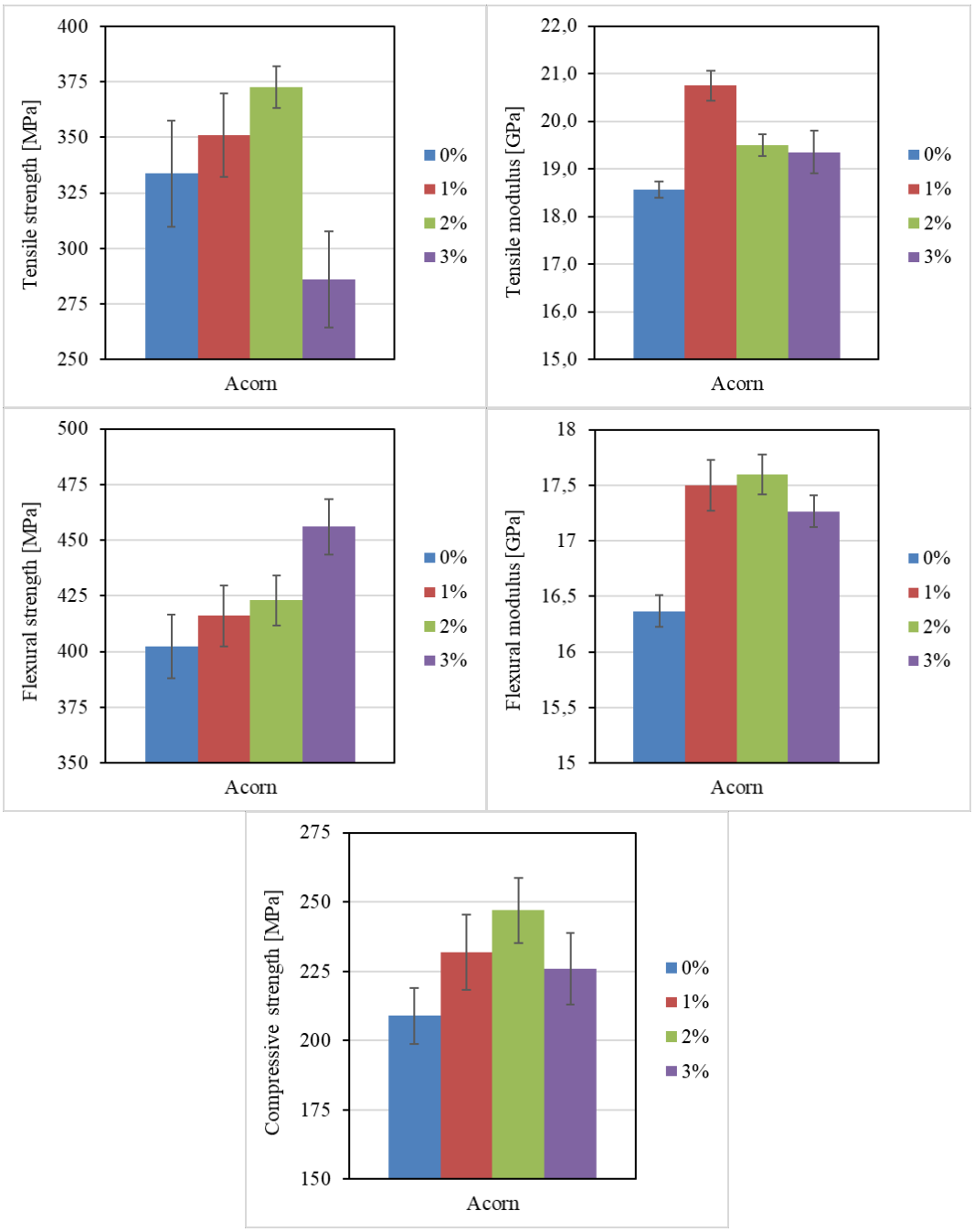

Figure 6. Mechanical strengths and mechanical modulus of acorn reinforcement specimens

Force – deformation curves obtained from the quasi-static punch-shear tests of 0%, 1%, 2% and 3% particle reinforced composites are shown in Figure 7. It can be observe from the figure that, curves increase linear tendency at the beginning of the test and initial parts of curves start separate further from each other along with increasing test speed. After initial area, curves turn to a nonlinear form because of permanent deformation damages. Curves continue to rising until plugging point. Force of composites decreases drastically after plugging point and stabilizes at a certain value after tip of cross-head move out from back of composite plate. After this point, friction create resistance effect against the cross-head.

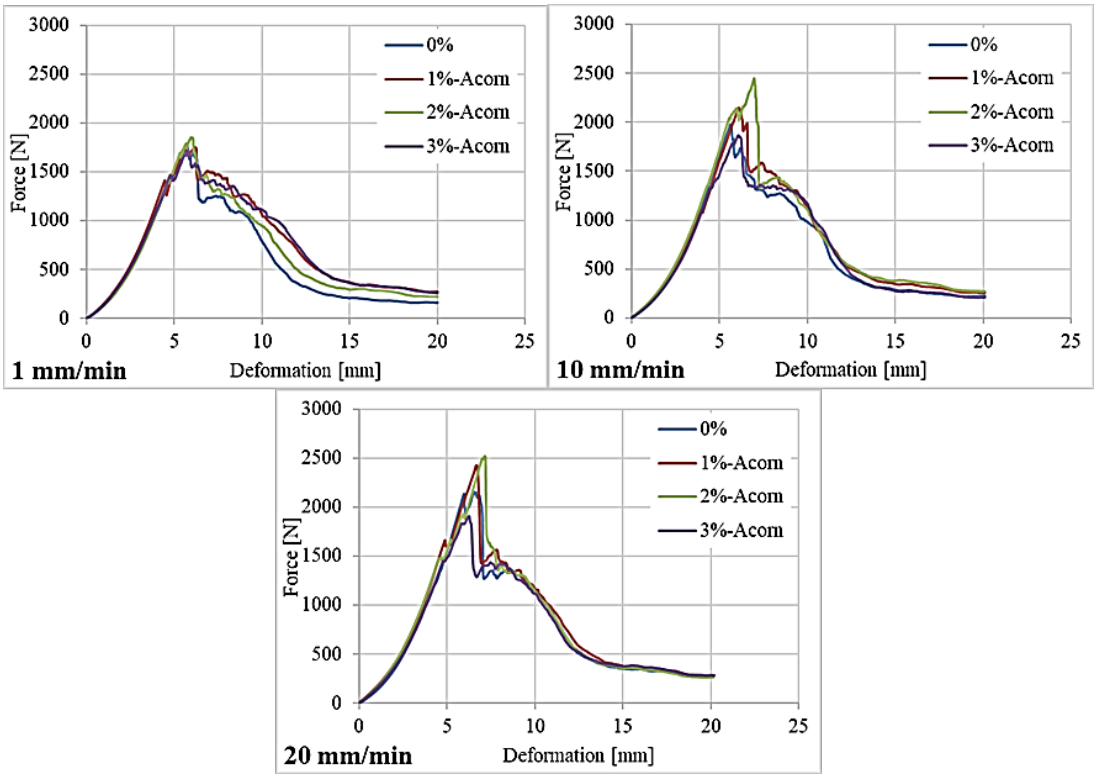

Figure 7. Force–Displacement curves of quasi-static punch-shear tests

In order to evaluate the quasi-static punch-shear strengths of particle-reinforced composites, maximum penetration force graphs and values are given in Table 2 and Figure 8. According to the Figure 8, maximum penetration forces of each composite group increases with increasing the test speed. Additionally, maximum penetration forces of composites gets higher values with higher particle reinforcement ratios until 2% particle ratio. Kılınc et al. determined that certain mechanical properties of composite, such as tensile strength, decrease when the ratio of the filler in the composite exceeds a certain value. They asserted that the reason for this situation was due to the poor distribution of the increased filler in the composite.

Table 2. Maximum penetration forces of quasi-static punch-shear tests

	0%	**1%**	**2%**	**3%**
1mm/min	1798	1845	1853	1755
10mm/min	2086	2178	2210	1892
20mm/min	2168	2267	2300	1943

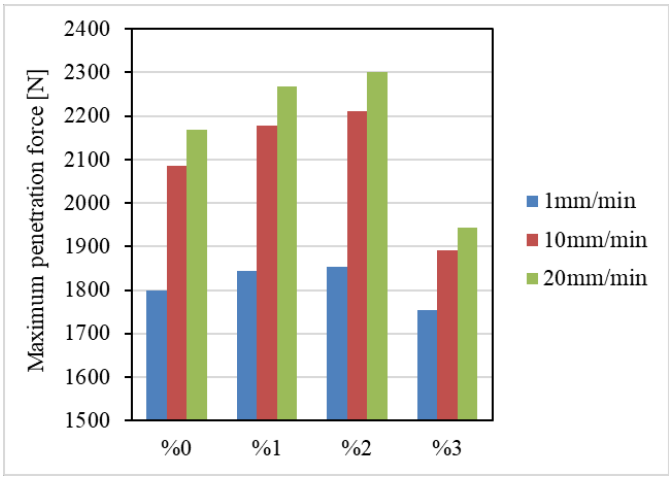

Figure 8. Maximum penetration forces of quasi-static punch-shear tests

Fiber plugging and rapture (maximum penetration force) point of composites is a critical point for quasi-static punch-shear tests (Öztoprak et al., 2022). Because of that, absorbed energy graphs and values of quasi-static punch-shear tests at fiber rapture point and at 20 mm deformation are given in Table 3 and Figure 9. It can be seen in Figure 9a that energy value of each composite group at fiber rapture point increases with increasing test speed. Furthermore, absorbed energy of composites at fiber rapture point gets higher values until 2% particle ratio. It can be seen in Table 3 and Figure 9b that absorbed energy value of each composite group increases when test speed increasing 1mm/min to 10mm/min. On the other hand, it starts to decrease when test speed increasing to 20mm/min.

Table 3. Absorbed energy value (J) of quasi-static punch-shear tests at fiber rapture point and 20mm deformation

Absorbed energy (J)		0%	1%	2%	3%
Rapture point	1mm/min	4.2	4.3	4.6	4.4
	10mm/min	5.5	5.9	6.6	4.8
	20mm/min	6.3	6.6	7.6	5.0
20mm	1mm/min	12.3	13.4	13.9	13.6
	10mm/min	15.2	15.3	15.4	14.8
	20mm/min	14.9	15.2	15.3	14.6

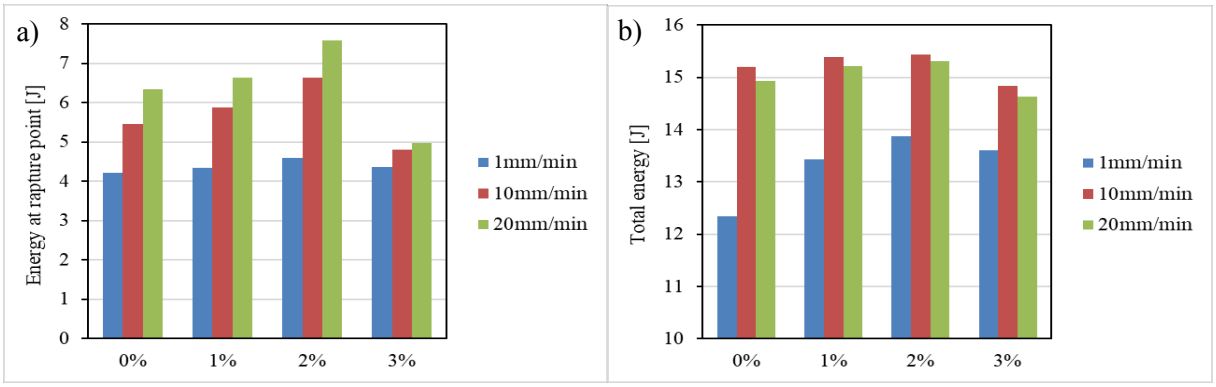

Figure 9. Absorbed energy of quasi-static punch-shear tests at a) fiber rapture point, b) 20 mm deformation

4. Conclusions

In this study, the effect of different amounts of acorn powder reinforcement on the mechanical and quasi-static penetration behavior of glass fiber reinforced composites was investigated experimentally. The quasi-static penetration tests were carried out at 1, 10 and 20 mm/min cross-head test speeds. The obtained conclusion can be summarized as:

- Tensile and compressive strengths of composites increase as the particle reinforcement increase up to 2%.
- Flexural strength of composites continuously increases with increasing particle ratio.
- Maximum penetration force of composites increases along with particle reinforcement up to 2% at quasi-static punch-shear tests.
- All absorbed energy values of composites decreases at 3% particle ratio.
- While the absorbed energy values obtained at fiber rapture point increase continuously with the increasing of test speed, absorbed energy value of composites at 20mm deformation decreases at 20mm/min test speed.

Acknowledgments

The first author would like to thank YÖK 100/2000 Program of The Higher Education Council for the support it received throughout his Ph.D. The first author would like to thank the 2211-A program (Grant Number: 1649B031902841) of The Scientific and Technological Research Council of Türkiye (TUBITAK) for providing support to his research at the Dokuz Eylül University.

Conflict of Interest

The authors declare no conflict of interest.

References

Agayev, S., & Ozdemir, O. (2019). Fabrication of High Density Polyethylene Composites Reinforced with Pine Cone Powder: Mechanical and Low Velocity Impact Performances. *Materıals Research Express,* 6(4), 045312.

Bledzki, A.K., & Jaszkiewicz, A. (2010). Mechanical Performance of Biocomposites Based on PLA and PHBV Reinforced with Natural Fibers—A Comparative Study to PP. *Composites Science and Technology,* 70(12), 1687-1696.

Bledzki, A.K., Mamun, A.A., & Volk, J. (2010). Barley Husk and Coconut Shell Reinforced Polypropylene Composites: the Effect of Fibre Physical, Chemical and Surface Properties. *Composites Science and Technology,* 70(5), 840-846.

Erkendirici, Ö., & Haque, B.Z. (2012). Quasi-static Penetration Resistance Behavior of Glass Fiber Reinforced Thermoplastic Composites. *Composites Part B,* 43, 3391-3405.

Essabir, H., Nekhlaoui, S., Malha, M., Bensalah, M.O., Arrakhiz, F.Z., Qaiss, A., & Bouhfid, R. (2013). Bio-composites based on Polypropylene Reinforced with Almond Shells Particles: Mechanical and Thermal Properties. *Materials & Design*, 51, 225-230.

Gama B.A., & Gillespie J.W. Jr. (2008.) Punch Shear Based Penetration Model of Ballistic Impact of Thick-Section Composites. *Composite Structures,* 86, 356–369.

Kılınç, A.C., Atagur, M., Ozdemir, O., Sen, I., Kucukdogan, N., Sever, K., Seydibeyoglu, O., Sarikanat, M., & Seki, Y. (2016). Manufacturing and Characterization of Vine Stem Reinforced High Density Polyethylene Composites. *Composites Part B: Engineering,* 91, 267–74.

Le Troedec, M., Sedan, D., Peyratout, C., Bonnet, J.P., Smith, A., Guinebretiere, R., Gloaguen, V., & Krausz, P. (2008). Influence of Various Chemical Treatments on the Composition and Structure of Hemp Fibres. *Composites Part A,* 39, 514–22.

Öztoprak, N., Özdemir, O., & Kanda, H. (2022). Quasi-static Perforation Response of Inter-ply Hybrid Polypropylene Composites at Various Temperatures. *Journal of Composite Materials,* 56(3), 359–371.

Sadeghi, M., & Pol, M.H. (2019). Investigation of Behaviors of Glass/Epoxy Laminate Composites Reinforced with Carbon Nanotubes under Quasi-static Punch Shear Loading. *Journal of Sandwich Structures and Materials,* 21(4), 1535-1556.

Singh, K.K, & Rawat P. (2018). Mechanical Behavior of Glass/Epoxy Composite Laminate with Varying Amount of MWCNTs under Different Loadings. *Materials Research Express,* 5(5), 055012.

Taghizahed, S.A., Liaghat, G., Niknejad, A., & Pedram, A. (2018). Experimental Study on Quasi-static PenetrationP of Cylindrical Indenters with Different Nose Shapes into the Hybrid Composite Panels. *Journal of Composite Materials,* 53(1), 107-123.

Zahedi, M., Pirayesh, H., Khanjanzadeh, H., & Tabar, M.M. (2013). Organo-modified Montmorillonite Reinforced Walnut Shell/Polypropylene Composites. *Materials & Design,* 51, 803-809.